Biomass-derived carbon material as efficient electrocatalysts for the oxygen reduction reaction

Cao, Yue; Sun, Yegeng; Zheng, Runtian; Wang, Qing; Li, Xue; Wei, Haoran; Wang, Likai; Li, Zhongfang; Wang, Fagang; Han, Ning

Published in:
Biomass and Bioenergy

DOI:
10.1016/j.biombioe.2022.106676

Publication date:
2023

Document Version
Publisher's PDF, also known as Version of record

Biomass and Bioenergy 168 (2023) 106676

Contents lists available at ScienceDirect

Biomass and Bioenergy

journal homepage: www.elsevier.com/locate/biombioe

Biomass-derived carbon material as efficient electrocatalysts for the oxygen reduction reaction

Yue Cao [a,1], Yegeng Sun [a,b,1], Runtian Zheng [c], Qing Wang [a], Xue Li [d], Haoran Wei [e], Likai Wang [d], Zhongfang Li [d], Fagang Wang [a,*], Ning Han [f,**]

[a] School of Material Science and Engineering, Shandong University of Technology, Zibo, 255000, China
[b] Shandong Sunway Chemical Group Co., Ltd, Zibo, 255000, China
[c] Laboratory of Inorganic Materials Chemistry (CMI), University of Namur, 61 rue de Bruxelles, B-5000, Namur, Belgium
[d] School of Chemistry and Chemical Engineering, Shandong University of Technology, Zibo, 255000, China
[e] Department of Electrical and Computer Engineering, University of Texas at Dallas, Richardson, TX, 75080, USA
[f] Department of Materials Engineering, KU Leuven, Kasteelpark Arenberg 44, 3001, Leuven, Belgium

ARTICLE INFO

Keywords:
Oxygen reduction
Biomass
Carbon
Catalyst

ABSTRACT

Despite the abundance of carbon in nature, a significant portion of the existing biomass carbon materials in livestock, agriculture, and marine fishery industry are currently being wasted. Utilizing sustainable carbon materials as an alternative to noble Pt-based catalysts is crucial step to convert widely available and low-cost biomass resources into clean energy systems. Therefore, the rational synthesis of carbon-based catalysts for oxygen reduction reaction (ORR) has become a hot research focus in the field of electrochemistry. In this study, the recent progress in the synthesis of ORR electrocatalysts using sustainable biomass resources was reviewed; the activation and synthesis strategies of various biomass resources, as well as the microstructure and oxygen reduction performance of the prepared carbon-based catalysts were investigated. It is hoped that this review article will promote the understanding of various parameters from biomass as precursors for catalyst preparation and make contribute to the transition of biomass resources from the wasted carbon materials to the main catalysts in future energy devices.

1. Introduction

In view of the growing energy demand and the increasing concerns about environmental issues, significant importance has been attached to the renewable and clean energy [1–5]. Among the sustainable energy resources, wind energy and solar energy are of most abundance and easy availability [6,7]. However, such energy resources are highly dependent on climate, leading to great challenges for the efficient utilization of them [8–10]. Hence, in order to realize the efficient utilization of clean energy, it is urgent to develop fuel cell, battery, supercapacitor and other novel energy equipment [11–14], among which fuel cells have attracted great attention because of their wide applications [15–18]. ORR, as the core of fuel cell devices, determines the efficiency of energy conversion and storage [19–24]. However, ORR is slow in operation, and it requires precious metal catalysts (e.g., platinum) [25–29]. Thus, the scarcity, poor stability and high cost of Pt-based ORR catalysts have hindered the commercial application of fuel cells [30–34]. Therefore, it is crucial to find alternative ORR catalysts which are not only earth-abundant and low cost, but also of high catalytic activity [35–39]. Porous carbon materials have been studied widely because of their excellent electrical conductivity [40,41], tunable morphology [42], high surface area [43], abundant precursors [8], and chemical and structural stability [44]. Despite the promising catalytic activities of carbon nanotubes, graphene, and other carbon materials, their large-scale commercialization is limited due to the excessive cost and synthesis processes [45–47]. Therefore, the advanced carbon-based catalysts derived from biomass resources have received extensive attention (see Table 1).

Carbon can combine with other elements such as nitrogen, oxygen, hydrogen and sulfur to provide energy and structural tissue for living organisms in the biosphere [48,49]. Biomass resources are classified into

* Corresponding author.
** Corresponding author. Department of Materials Engineering, KU Leuven, Kasteelpark Arenberg 44, 3001, Leuven, Belgium.
E-mail addresses: a_gang@sdut.edu.cn (F. Wang), ning.han@kuleuven.be (N. Han).
[1] Yue Cao, Yegeng Sun are co-first authors.

https://doi.org/10.1016/j.biombioe.2022.106676
Received 8 June 2022; Received in revised form 5 November 2022; Accepted 27 November 2022
Available online 18 December 2022

Table 1
ORR electrocatalysts obtained from biomass.

Biomass source	Other precursors	Synthesis strategy	Surface area ($m^2\ g^{-1}$)	Pore volume ($cm^3\ g^{-1}$)	E_{Onset}	$E_{1/2}$	Electrolyte	Reference
Shrimp shells	Pyrrole and $FeCl_3$	HTC, Pyrolysis	806.7	0.205	−0.017 V *vs.* Ag/AgCl	−0.15 V *vs.* Ag/AgCl	0.1 M KOH	[80]
Soybean	$ZnCl_2$	Activation, pyrolysis and graphitization	949	–	−0.02 V *vs.* Ag/AgCl	−0.12 V *vs.* Ag/AgCl	0.1 M KOH	[93]
Shrimp shells	–	HTC, Silica templating and pyrolysis	360.2	–	−0.06 V *vs.* Ag/AgCl	−0.21 V *vs.* Ag/AgCl	0.1 M KOH	[101]
Duck blood	$FeCl_3{\cdot}6H_2O$	Pyrolysis, ball milling and pyrolysis	–	–	0.002 V *vs.* Ag/AgCl	0.137 V *vs.* Ag/AgCl	0.1 M KOH	[103]
Pig blood (PB)	$FeCl_3{\cdot}6H_2O$	Carbonization, ball milling, acid leaching and pyrolysis	641	–	−0.04 V *vs.* Ag/AgCl	−0.16 V *vs.* Ag/AgCl	0.1 M KOH	[51]
Blood protein	Vulcan XC-72R	Pyrolysis, ball milling, pyrolysis, acid leaching and pyrolysis again	93	0.18	0.90 V *vs.* RHE	0.78 V *vs.* RHE	0.1 M KOH	[107]
Cattle bone	Co_3O_4	Precarbonized, mixed with Co $(OAc)_2$, centrifuging, washing and drying	1070	–	0.960 V *vs.* RHE	0.853 V *vs.* RHE	0.1 M KOH	[108]
Eggs	–	Stirring with TEOs, precarbonized and anneal	970	–	0.84 V *vs.* RHE	0.69 V *vs.* RHE	0.1 M KOH	[112]
Eggs	$FeCl_3{\cdot}6H_2O$, multi-walled carbon nanotubes (MWNT)	Mixed with $FeCl_3{\cdot}6H_2O$ and MWNT, pyrolysis and pyrolysis again	680	–	−0.007 V *vs.* Ag/AgCl	−0.133 V *vs.* Ag/AgCl	0.1 M KOH	[113]
Egg-yolk	g-C_3N_4	Grind and pyrolysis	447	–	0.89 V *vs.* RHE	–	0.1 M KOH	[114]
Human hair	NaOH	Precarbonized, activation and pyrolysis	1814	–	−0.016 V *vs.* Ag/AgCl	–	0.1 M KOH	[116]
Human urine	–	Drying and pyrolysis	811	–	−0.03 V *vs.* Ag/AgCl	–	0.1 M KOH	[117]
Biomass source	Other precursors	Synthesis strategy	Surface area ($m^2\ g^{-1}$)	Pore volume **($cm^3\ g^{-1}$)**	E_{Onset}	$E_{1/2}$	Electrolyte	Reference
Porphyra	$FeCl_3{\cdot}6H_2O$	Grind and pyrolysis	1533.7	0.39	0.96 V *vs.* RHE	0.84 V *vs.* RHE	0.1 M KOH	[118]
Porphyra	Hemin	Activation and carbonization and pyrolysis	1301.5	197.6	–	0.87 V *vs.* RHE	0.1 M KOH	[119]
Catkins	$FeCl_3$, KOH and melamine	Stir, pyrolysis and acid leaching	461.5	–	−0.098 V *vs.* Ag/AgCl	−0.194 V *vs.* Ag/AgCl	0.1 M KOH	[120]
Tofu	Na_2PdCl_4, $HAuCl_4$ and $H_2PtCl_6{\cdot}6H_2O$	Activation, carbonization and pyrolysis	3814	2.08	1.04 V *vs.* RHE	0.91 V *vs.* RHE	0.1 M $HClO_4$	[106]
Tofu	Urea and NaCl	Pyrolysis	988.2	0.689	0.96 V *vs.* RHE	0.81 V *vs.* RHE	0.1 M KOH	[123]
Pomelo peel	$Co(NO_3)_2{\cdot}6H_2O$ and KOH	Activation and pyrolysis	–	1.28	0.87 V *vs.* RHE	0.78 V *vs.* RHE	0.1 M KOH	[125]
Peanut shells	$Co(OH)_2$ and NaH_2PO_2	Precarbonized, CO_2 reduction	671.4	–	0.91 V *vs.* RHE	0.81 V *vs.* RHE	0.1 M KOH	[74]
Coconut shell	NH_4F and dicyandiamide	Carbonization, activation and pyrolysis	1028.3	0.83	0.985 V *vs.* RHE	0.834 V *vs.* RHE	0.1 M KOH	[131]
Corn silk	$FeCl_3$ and KOH	HTC, precarbonized and pyrolysis	1038.9	0.83	0.957 V *vs.* RHE	0.852 V *vs.* RHE	0.1 M KOH	[133]
D-Glucose and Cellulose	Soya bean flour	HTC, freeze drying and pyrolysis	449	0.25	−0.06 V *vs.* RHE	–	0.1 M KOH	[138]
Glucose	NH_3, and thiophene	Silica templating, pyrolysis, heteroatoms doping, ammoxidation	1023	0.973	0.92 V *vs.* RHE	–	0.1 M KOH	[139]
Glucose	Dicyandiamide and $FeSO_4{\cdot}7H_2O$	Silica templating and pyrolysis	906.3	2.89	0 V *vs.* Ag/AgCl	−0.15 V *vs.* Ag/AgCl	0.1 M KOH	[140]
Glucose	Melamine and $FeSO_4{\cdot}7H_2O$	Pyrolysis	393	0.99	0.874 V *vs.* RHE	–	0.1 M KOH	[141]
Glucose	Prussian blue (PB)	Grind and pyrolysis	418	–	−0.055 V *vs.* Ag/AgCl	−0.152 V *vs.* Ag/AgCl	0.1 M KOH	[142]
Corn starch	Urea	Pyrolysis	1568.85	–	−0.03 V *vs.* Ag/AgCl	−0.15 V *vs.* Ag/AgCl	0.1 M KOH	[143]
Starch	Flake graphite, $FeCl_3$ and KSCN	HTC and pyrolysis	749.5	–	0.95 V *vs.* RHE	0.83 V *vs.* RHE	0.1 M KOH	[63]
Biomass source	Other precursors	Synthesis strategy	Surface area ($m^2\ g^{-1}$)	Pore volume **($cm^3\ g^{-1}$)**	E_{Onset}	$E_{1/2}$	Electrolyte	Reference
Chitin	–	Pyrolysis	526	–	0.054 V *vs.* Ag/AgCl	–	0.1 M KOH	[145]
Chitin	$ZnCl_2$	HTC, pyrolysis, activation and pyrolysis	300.7	0.31	−0.15 V *vs.* SCE	–	0.1 M KOH	[148]
Chitosan	$Fe(NO_3)_3{\cdot}9H_2O$, TiO_2 and NaOH	Stirring, pyrolysis and wash	1190	1.10	−0.01 V *vs.* Ag/AgCl	–	0.1 M KOH	[149]
Chitosan	$FeCl_3$	Pyrolysis	543	–	−0.08 V *vs.* Ag/AgCl	–	0.1 M KOH	[150]

(*continued on next page*)

animal biomass, plant (lignocellulose) biomass, as well as carbohydrates and polysaccharides [50]. Animal biomass includes animal waste, such as blood [51], excrement, feathers [52,53], and human feces, hair [54], and so on. Lignocellulose biomass, including soybean shell [55], eggplant [56], seaweed [57], leaves and grasses [58] and so on, is mainly generated through photosynthesis [59]. Carbohydrates and polysaccharides mainly include fructose [60,61], glucose [62] and its derivatives, starch [63], chitin [64], etc. Large amounts of biomass from human activities, agriculture, and marine fishing are wasted, which causes certain ecological impacts, greenhouse gas emissions and an increasing waste-management burden [65–67]. Therefore, it makes sense to convert sustainable biomass into advanced carbon-based materials. In addition, such advanced carbon-based materials play a significant role as oxygen reduction catalysts in new energy technologies [33,68–72]. The natural structure and rich elemental composition of biomass materials provide the carbon-based catalysts with porous structures [73–75] as well as abundant heteroatom doping [8], and also they can fully expose the active sites [76], which can enhance the catalytic activity. Therefore, numerous studies have focused on porous carbon-based materials and their applications in ORR [156–158]. Herein, we aspire to promote the selection of targeted biomass resources and the optimization of carbon-based material structures, so as to accelerate the development of highly active oxygen reduction catalysts.

Here, we outline the recent progress in oxygen reduction catalysts using biomass resources as precursors. Sections 2 and 3 describe in detail the synthetic strategies of matter-derived carbon nanomaterials including activated pore-making strategies, the physicochemical structures and oxygen reduction activity from plants, animals and Carbohydrates and polysaccharides. Finally, we offered personal views and recommendations on the synthesis of biomass carbon.

2. Synthetic method

2.1. Hydrothermal carbonization

Hydrothermal carbonization (HTC) is an environmentally friendly preparation method that converts biomass to practical carbon materials through dehydration, condensation, polymerization and other processes [50,77–79]. HTC is carried out in a mild aqueous medium below 200 °C, and the prepared carbon materials need to be further activated and pyrolysis to increase their pore volume and specific surface area (SSA).

Zhang et al. prepared N-doped carbon nanodots (N-CNs) using shrimp shells as precursors by a simple hydrothermal carbonization process, and then polymerized pyrrole in $FeCl_3$ solution and to obtain carbonized at high temperature to obtain Fe–N-PGC-800 (Fig. 1A) [80]. It can be clearly seen that pyrolysis in high temperature results in the conversion of pyrrole nitrogen to pyridine nitrogen. The prepared Fe–N-PGC-800 material exhibited a large SSA of 806.7 $m^2\ g^{-1}$ and presented a mesoporous structure, which contributed to the improvement of ORR performance. Gao et al. used willow leaf as carbon source to obtain bifunctional N-doped carbon quantum dots (N-CDs) by a green and environmentally friendly hydrothermal carbonization process (Fig. 1B) [81]. According to TEM images, N-CDs was very uniform with a diameter of about 2–4 nm. The supernatant (SP1) showed intense fluorescence under ultraviolet irradiation, which could be used as fluorescent ink. The catalyst (SP2) by pyrolysis had outstanding ORR activity and good durability.

2.2. Chemical and physical activation

Chemical activation usually involves impregnating biomass precursors with K_2CO_3, KOH, NaOH and $ZnCl_2$ solutions, etc., followed by pyrolysis and final pickling to remove chemical reagents [82–86]. The synthesis of porous carbon materials using the physical activation method is divided into two steps. First, initial carbonization is performed in an inert environment such as N_2 and Ar, and then activated at a high temperature of 600–1000 °C using N_2, CO_2, etc [73,87–90]. The activation method can be very successful in increasing the surface area and pore volume of biomass carbon materials, and their porosity can be well controlled [91].

Quan et al. prepared porous carbon catalysts by HTC and chemical activation method using osmanthus fragrans and sterchilia scaphigera as carbon sources, labeled as OPC and SPC, respectively [92]. OPC had a Tremella-like structure, dominated by micropores; while SPC had a honeycomb-like structure, dominated by mesopores (Fig. 1E and F). Besides, high-performance carbon-based catalysts were obtained by carbonizing soybean at high temperature with $ZnCl_2$ as an activated pore-forming agent [93]. It was shown that the BET SSA (949 $m^2\ g^{-1}$) of the catalyst can be significantly increased due to the activation of $ZnCl_2$, so that it had a higher active center density, which helped to improve the catalytic activity.

2.3. Hard and soft templating

Ordered inorganic solids such as mesoporous silica [94–98] are used as sacrificial hard template to guide the formation of pores during high temperature pyrolysis. However, the hard templating method has the following disadvantages. First, template must be removed using NaOH, HF and other toxic chemicals [99,100]. In addition, control over the pore diameter of porous material is also limited to the pores row of carbons that adopt the inverse structure of template pores. To avoid the use of toxic chemicals, soft templates is a good choice for preparing porous carbon materials. Soft template methods involve co-assembly between carbon precursors and surfactants in solution.

Liu et al. successfully reported a three-dimensional (3D) N-doped porous carbon (NPC) derived from low cost shrimp shells through simple SiO_2 spheres assisted, high temperature pyrolysis and HF acid leaching (Fig. 1G) [101]. It was found that the average pore size of three (3D) NPC was about 200 nm due to the removal of silica, and the carbon wall of 3D NPC exhibited an unusually distortional graphitic carbon lattice structure (Fig. 1H and I), indicating that more defects were formed in 3D NPC, thereby contributing to the enhanced electrocatalytic activity. Liu et al. developed N-doped porous carbon ORR catalyst (N-HPCMs) based on chelation-assisted multicomponent co-assembly strategy using banana peels as precursors and aluminum matrix composites and Pluronic F127 as co-templates (Fig. 1J) [102]. The N-HPCMs had many obvious three-dimensional mesoporous and microporous structures after HF treatment. It was found that this chelation-assisted multicomponent co-assembly strategy can tune the SSA and pore volume of N-HPCMs by simply changing the doses of Al^{3+} and F127.

Table 1 (*continued*)

Biomass source	Other precursors	Synthesis strategy	Surface area ($m^2\ g^{-1}$)	Pore volume ($cm^3\ g^{-1}$)	E_{Onset}	$E_{1/2}$	Electrolyte	Reference
Chitosan	Triphenyl phosphine and $FeCl_3$	HTC and pyrolysis	845	0.66	−0.014 V *vs.* AgCl	–	0.1 M KOH	[151]
Chitosan	$Co(Ac)_2$ and urea	Stirring, pyrolysis and wash	337	–	–	0.839 V *vs.* RHE	0.1 M KOH	[154]
Chitosan	$C_4H_6CoO_4{\bullet}4H_2O$ and $Mg(OH)_2$	Freeze drying, pyrolysis and pyrolysis again	1716	1.55	−0.075 V *vs.* AgCl	−0.151 V *vs.* AgCl	0.1 M KOH	[155]

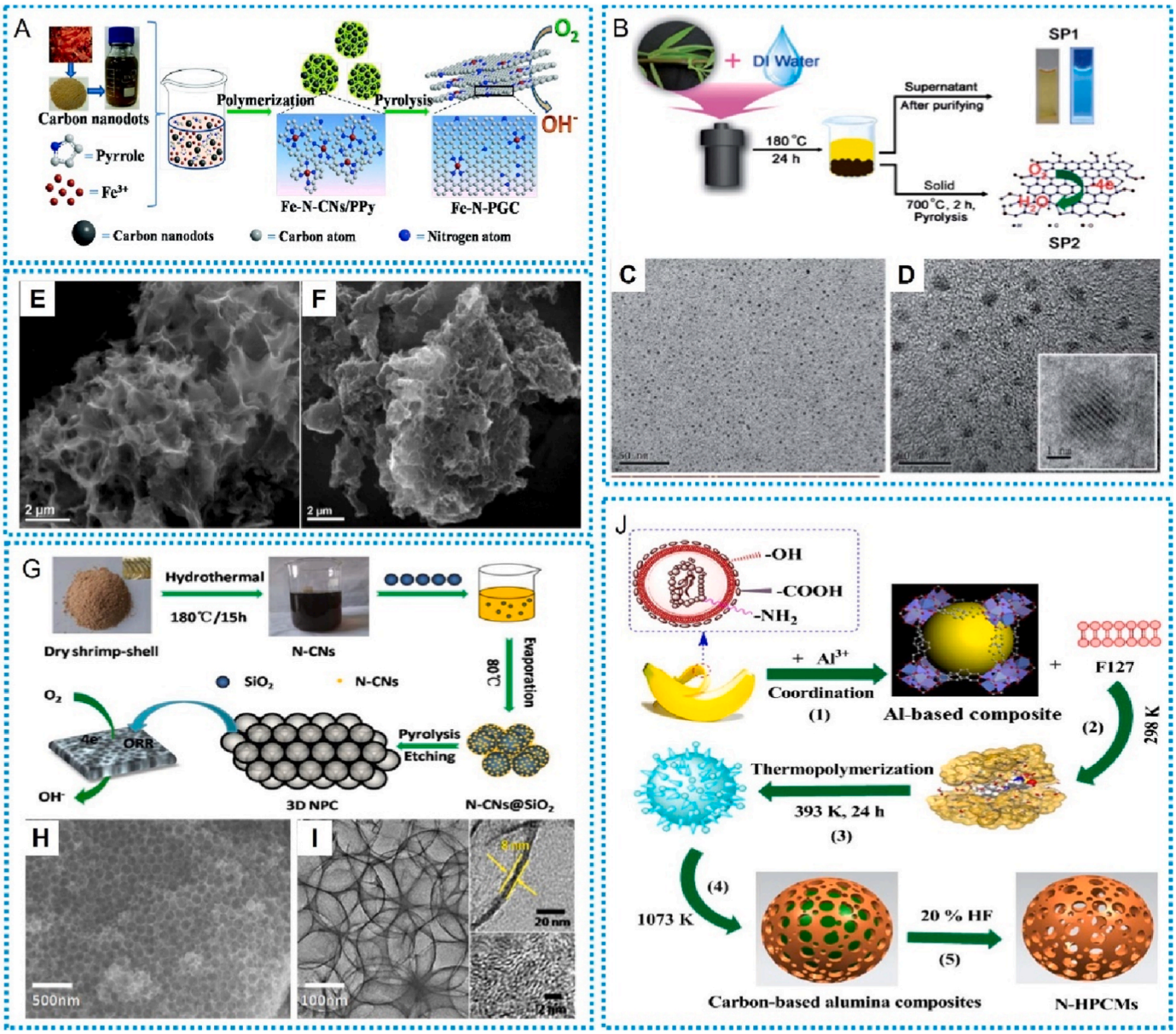

Fig. 1. (A) Synthesis procedure of Fe–N-PGC catalyst [80]. (B) Schematic procedure to obtain dual-function N-CDs using willow leaf as precursor system [81]. (C, D) TEM of the N-CDs material. (E, F) SEM of OPC and SPC materials [92]. (G) Synthesis procedure of three-dimensional NPC using low cost shrimp shells as precursor [101]. (H) SEM and (I) TEM of 3D NPC. (J) Schematic procedure to obtain N-HPCMs [102].

3. Biomass-derived carbon material as ORR electrocatalysts

3.1. Animal-based ORR electrocatalysts

Animals, including shrimp, fish, pigs and their waste (horns, blood, excrement, skins, bones, skins, cocoon silk) and human waste (hair and urine), etc., can be used to prepare carbon-based catalysts. These huge amounts kinds of biomass generated everyday which put enormous pressure on the environment. Rational use of this renewable energy is essential for ecological protection, waste management, and economic considerations. Considering that the ORR performance of catalysts can be enhanced by introducing dopants during post-processing, strategies for synthesizing oxygen reduction catalysts from various parts in animals, as well as their carbon structure and ORR performance, were described in detail in this chapter.

Blood proteins that are usually discarded as waste include abundant hemoglobin.

Duck blood is a waste produced from the process of slaughtering ducks to prepare the Fe-doped carbon materials (CDB-Fe) for ORR [103]. Hemoglobin itself contains catalytically Fe active centers. CDB-Fe was composed of many irregular particles with diameters between 200 nm and 500 nm, shown in Fig. 2A and B. With the presence of Fe, the increased nitrogen and pyridinic N content of CDB-Fe suggested that the successful doping of Fe contributed to the increase of nitrogen content and the change of coordination ratios of various C–N bonds. The onset potential and half-wave potential of ORR for CDB-Fe were 2 mV and 137 mV, respectively, which were comparable to the performance of Pt/C catalyst (Fig. 2C and D).

Pig blood can be used to synthesize porous carbon materials and serve as an electrocatalyst. Pig blood is a sustainable animal resource which is rich in nitrogen due to its high protein content. Maruyama et al. obtained an catalyst using animal hemoglobin of oxygen reduction for a proton exchange membrane (PEM) fuel cell [104]. Catalytic performance was significantly enhanced by a two-step carbonization pyrolysis. In addition, the catalytic activity was much higher in the carbonization atmosphere of CO_2/Ar (25:75) mixed gas than that in pure air. First, this

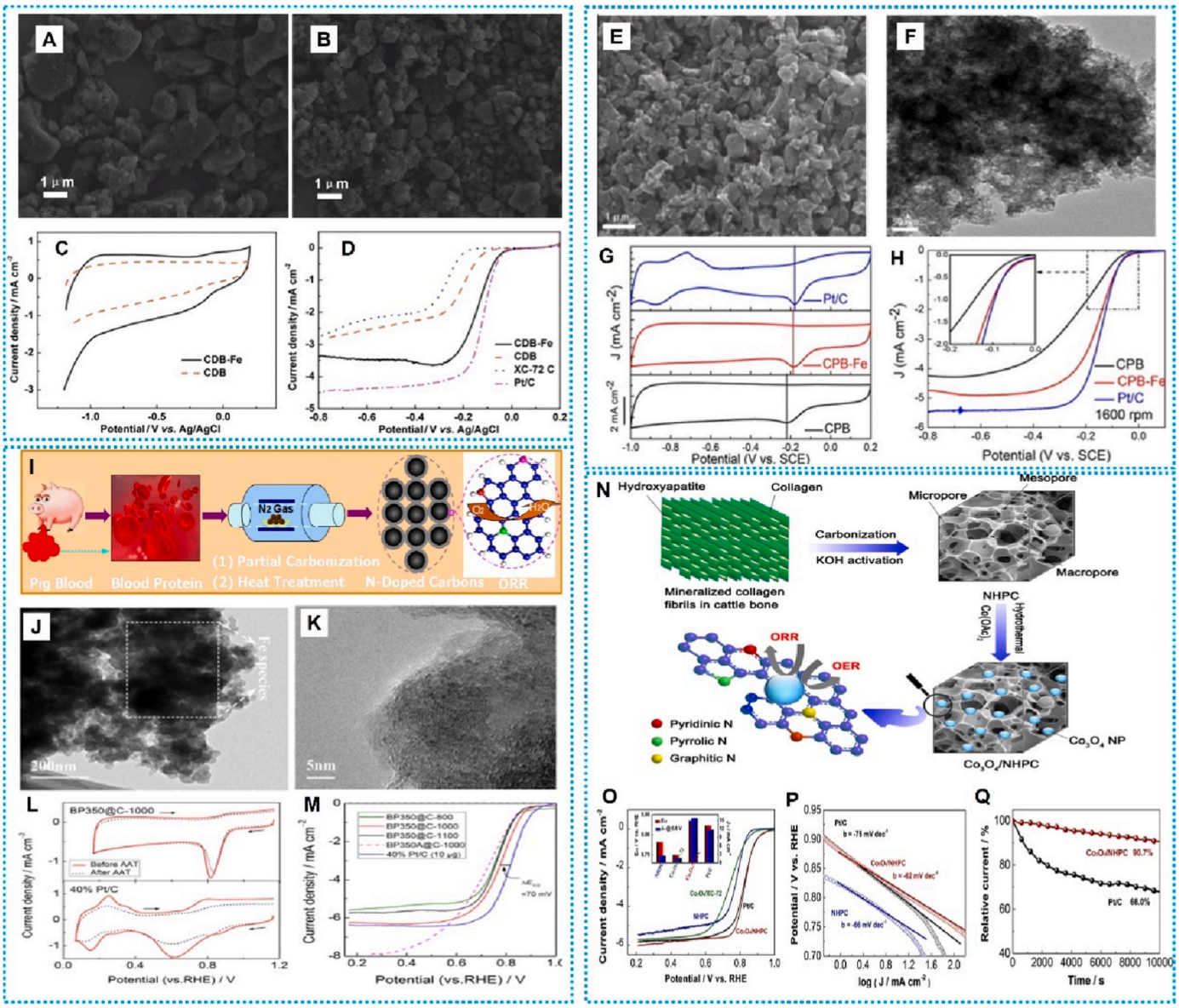

Fig. 2. (A, B) SEM of carbon materials from duck blood before and after iron treatment, respectively [103]. (C) CV curves and (D) LSV curves of CDB-Fe catalyst in 0.1 mol L^{-1} KOH solution. (E) SEM and (F) TEM of pig blood-derived carbon material [51]. (G) CV curves and (H) LSV curves of CPB-Fe and Pt/C catalysts. (I) Schematic diagram of the synthesis of N–CNS using blood proteins as precursors [107]. (J) TEM and (K) HR-TEM images of BP350@C-1000. (L) CV curves and (M) LSV curves of these catalyst. (N) Schematic procedure to obtain the Co_3O_4/NHPC ORR catalyst [108]. (O) LSV curves of Co_3O_4/NHPC and Pt/C catalyst in O_2-saturated 0.1 M KOH solution. (P) Tafel plots of these electrocatalysts. (Q) The i-t chronoamperometry curves of Co_3O_4/NHPC and Pt/C catalyst.

enhanced the SSA and pore volume of the carbonized material, making it easier to expose catalytically active sites, and second, it could converted Fe^{3+} to Fe^{2+}, which acted as oxygen bonding sites in the ORR.

Some biomass itself contains catalytic active centers, which can be used not only as carriers but also directly as catalysts. The presence of Fe in the carbonization process profoundly affected the degree of graphitization, formation of pyridinic N, and ORR catalytic activity of the prepared electrocatalyst. Later Zhang et al. successfully prepared a N self-doped carbon electrocatalyst with the aid of metal iron based on pig blood (Fig. 2E and F) [51]. The contents of pyridine N and graphite N of Fe-free catalyst (CPB) were 30.1% and 39.4%, respectively, while those of Fe-containing catalyst (CPB–Fe) were 35.1% and 39.2%, respectively. The limited current density (J_L) can be improved with graphitic N of ORR catalyst, while the onset potential (E_{onset}) can be enhanced with pyridinic N [105,106]. CPB exhibited an obvious ORR peak for ORR at −0.22 V *vs.* Ag/AgCl. After iron was added to PB, the ORR peak of CPB-Fe moved to a higher positive potential at −0.19 V. Besides, CPB-Fe showed a positive E_{onset} (−0.04 V *vs.* Ag/AgCl) and half-wave potential ($E_{1/2}$) of −0.16 V *vs.* Ag/AgCl, which were comparable to those of commercial Pt/C catalyst (Fig. 2G and H).

Chen successfully prepared an ORR electrocatalyst by using blood protein and carbon nanospheres at different pyrolysis temperatures (Fig. 2I) [107]. As shown in Fig. 2J and K), many Fe-containing agglomerations and an amorphous structure were shown in BP350@C-1000, indicating more structural defects and more exposed edges can be formed, which was conducive to the improvement of oxygen reduction activity. In the pyrolysis process, the metallic Fe of raw blood protein can enhance the conversion of oxidative N to planar N, as well as the co-incorporation of pyridine and pyrrolic N groups into the carbon material, which further generated more defects in the carbon structure. Pyridine and pyrrolic N may be the most influential N functional groups on ORR activity and can serve as the ORR active sites of catalysts. In conclusion, the catalyst had outstanding catalytic activity for ORR (Fig. 2L and M).

As a kind of biomass waste, animal bones such as fish scales [109, 110], pig bones and cow bones [108,111], are widely used as low-cost carbon sources to obtain carbon materials. Collagen in animal bones can provide C and N resources to synthesize heteroatom-doped carbon materials, while hydroxyapatite crystals can serve as hard templates to generate pore structures, therefore bones can be pyrolyzed into carbon precursors for ORR. Carbon materials with high content of N doping and typical 3D hierarchical porous structures can be produced. Co_3O_4 nanoparticles anchored on N-doped 3D hierarchically porous carbon material with (Co_3O_4/NHPC) as an high-efficiency ORR catalyst derived from cattle bone can be obtained through a simple hydrothermal synthesis process (Fig. 2N) [108]. The high SSA of Co_3O_4/NHPC as high as 1070 $m^2\ g^{-1}$, hierarchical porous structure and high content of N doping (4.93 wt %) facilitated the uniform anchoring of Co_3O_4 nanoparticles on the carbon support and enhanced the mass transfer capacity. Notably, the Co_3O_4/NHPC catalyst exhibited outstanding ORR activity. The $E_{1/2}$ was 0.853 V *vs*. RHE, the tafel slope was 63 mV dec^{-1}, and after a test lasting for 10 000 s, the relative current loss was only 1.74% (Fig. 2Q).

Eggs are rich in protein, cholesterol and lecithin, etc., which can be used as precursors of carbon and nitrogen. Wu et al. synthesized nitrogen, phosphorus-doped carbon microspheres with mesoporous structure (egg-CMS) by a hard templating method, using eggs as carbon precursors through a spray-drying process, pyrolysis, and template removal (Fig. 3AC) [112]. The prepared carbon microspheres had regular mesoporous structure and large SSA (970 $m^2\ g^{-1}$). When prepared as an oxygen reduction catalyst, the egg-CMS catalyst had a large limiting current (4.36 mA cm^{-2}), a positive $E_{1/2}$ (0.84 V *vs*. RHE), shown in Fig. 3D. In terms of stability, 92% of the initial current can be maintained after 20 h of testing (Fig. 3E). It is demonstrated that the egg-CMS catalyst can be used in fuel cells.

Zhang et al. synthesized Fe and N doped carbon materials (CE-Fe-MWNT) used eggs as the N source and carbon source, transition metal iron as the iron source, combined with multi-walled carbon nanotubes (MWNT), by cooking denaturation and secondary heat treatment [113]. TEM showed that the carbon material obtained by high-temperature pyrolysis can be well combined with MWNTs and had a porous

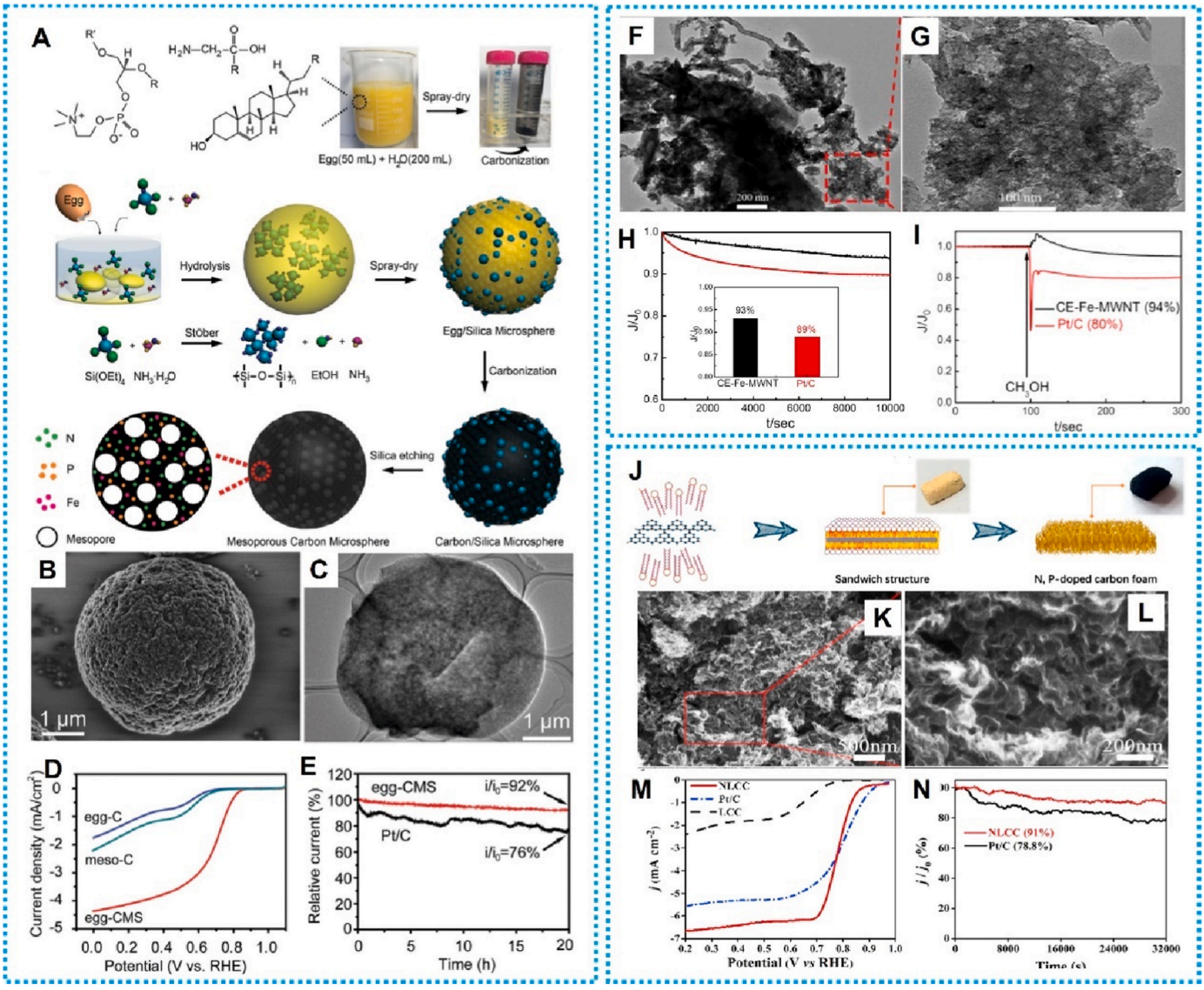

Fig. 3. (A) Schematic diagram of preparation of egg-CMS by a hard templating method [112]. (B) SEM and (C) TEM of egg-CMS. (D) LSV curves of egg-CMS catalyst in O_2-saturated 0.1 M KOH solution. (E) The chronoamperometry curves of egg-CMS and Pt/C catalyst. (F, G) TEM images of the CE-Fe-MWNT material [113]. (H) The methanol tolerance curves of CE-Fe-MWNT and Pt/C catalyst. (I) Chronoamperometric responses of CE-Fe-MWNT and Pt/C catalyst after methanol introduction. (J) Schematic procedure to obtain NLCC by in-situ foaming technology [114]. (K, L) SEM image of NLCC. (M) LSV curves of NLCC catalyst. (N) The i-t chronoamperometry curves of NLCC and Pt/C catalyst.

structure (Fig. 3F and G), which was beneficial to promote ORR mass transfer and thus enhance ORR activity. The MWNTs with high graphitization acted as a stable matrix to immobilize ORR active sites because of its perfect electrical conductivity and stability. Electrochemical tests showed that the CE-Fe-MWNT catalyst had excellent ORR activity in alkaline electrolyte, outstanding stability (Fig. 3H) and methanol resistance (Fig. 3I), making it a viable alternative to expensive Pt-based catalysts. Xian et al. used crude lecithin extracted from eggs as a phosphorus source and C_3N_4 as a self-sacrificing template to obtain nitrogen and phosphorus-doped carbon materials (NLCC) by in-situ foaming technology (Fig. 3J) [114]. The unique structure of the lecithin molecule can encapsulate g-C_3N_4. During the pyrolysis, g-C_3N_4 could be decomposed, and the mixture was gradually expanded, and finally a special carbon foam composed of many multi-folded morphology nanosheets was formed (Fig. 3K and L). In alkaline electrolyte, the NLCC catalyst showed a significant J_L of 6.7 mA cm^{-2} (Fig. 3M), which was significantly greater than that of Pt/C catalyst (5.5 mA cm^{-2}). In terms of stability, after about 9 h of chronoamperometry, the NLCC catalyst only lost 9% of the current density, proving its excellent long-term durability (Fig. 3N).

Human hair is composed of α-keratin, containing 15–16% N and 4.5–5.5% S, which can be used to synthesize N, S doped carbon catalysts for ORR [115]. Kalaiselvi et al. activated pre-carbonized hair with NaOH and then pyrolyzed at high temperature to obtain hair-derived carbon materials (HCC) for anode materials of sodium-ion battery and cathode ORR catalysts [54]. Due to its unique structural characteristics and large number of heteroatoms, the HHC exhibited excellent rate performance and long-term cycling performance and when used in ORR, HCC catalyst showed good ORR performance and long-term durability (Fig. 4A and B).

Chaudhari et al. prepared N, S-doped carbon (HC-*X*, *X* represents the carbonization temperature) by pre-carbonization, NaOH activation, and high-temperature carbonization by using hair as nitrogen and sulfur sources (Fig. 4C) [116]. The unique preparation strategy including mild NaOH activation and further high-temperature graphitization enhanced the electrical conductivity of carbon materials and preserving valuable N, S heteroatoms. HC-900 as a catalyst exhibited excellent ORR performance, four-electron selectivity (electron transfer was between 3.80 and 3.90), and long-term stability (HC-900 lost 14% of current density after 50000 s), suggesting that hair-derived carbon materials can be promising alternatives to Pt/C catalysts (Fig. 4D–G). The author further proposed a "proof of concept" that used urine to produce a new type of carbon called "urine carbon" (URC) (Fig. 4H and I) [117]. High porosity can be created by removing the inherent salt particles in the URC materials, and multiple heteroatoms can be doped into URC materials via high-temperature carbonization without the use of complex and expensive templates and the addition of additional precursors of heteroatoms. Electrochemical tests showed that the mass activities of the URC-900 and URC-1000 were increased by 22% and 24%, respectively, compared with other catalysts. Surprisingly, URC-1000 had low BET surface area and less content of nitrogen, but still exhibited the outstanding ORR activity. This is due to lower resistivity, presence of numerous heteroatoms, high electrical conductivity and a large number of pore structures (Fig. 4J and K).

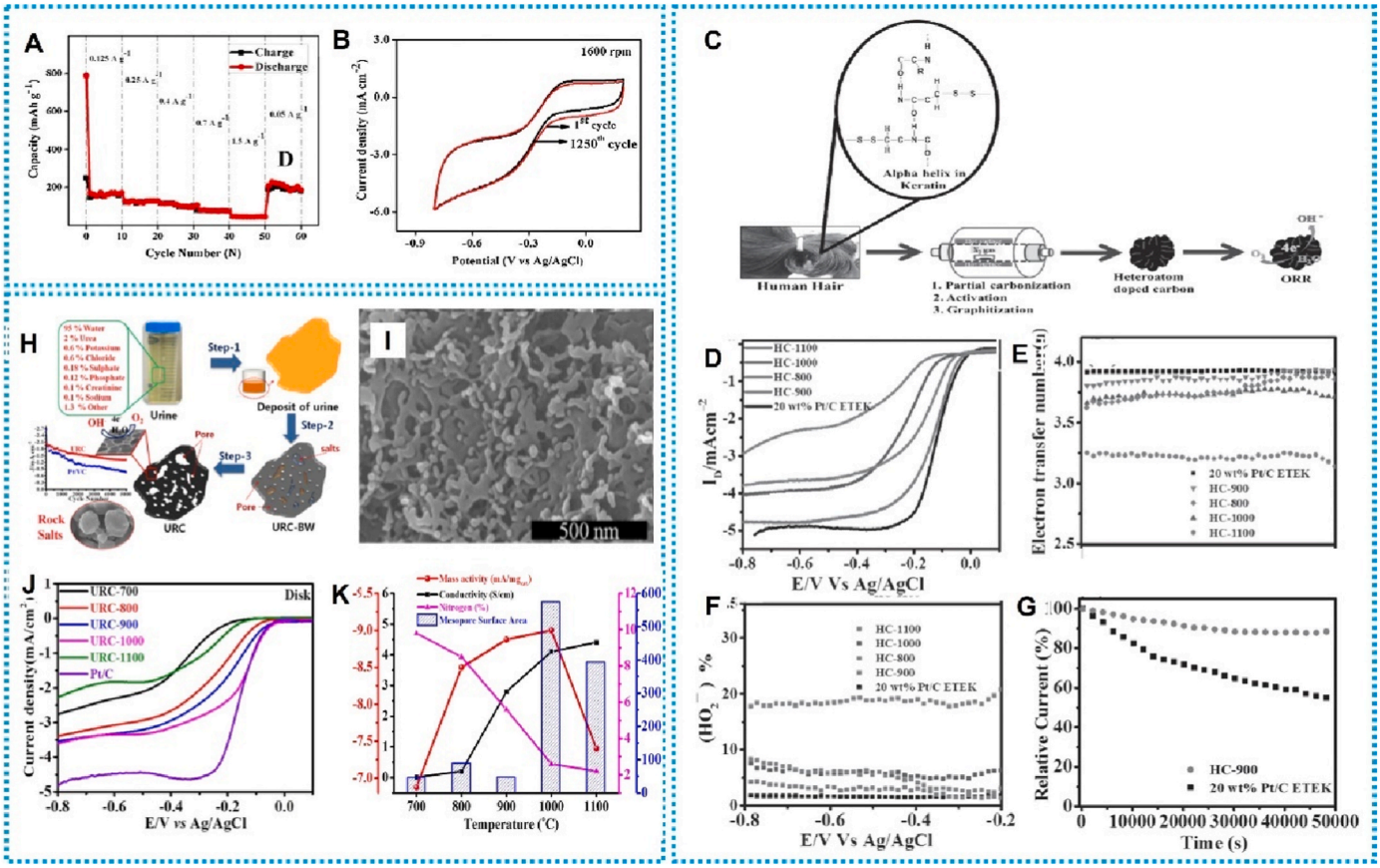

Fig. 4. (A) Rate performance behavior of HCC anodes [54]. (B) Durability test of HCC catalyst. (C) Schematic procedure to obtain N, S-doped carbon by using hair as nitrogen and sulfur sources [116]. (D) LSV curves of HC-*X* catalyst in 0.1 M KOH. (E) The electron number of HC catalyst at different pyrolysis temperatures. (F) Peroxide yield of HC catalyst at different pyrolysis temperatures. (G) The i-t chronoamperometry curves of HC-900 and Pt/C catalyst. (H) Schematic diagram of preparation of urine carbon (URC) [117]. (I) SEM image of URC-1000. (J) LSV curves of URC catalyst at different pyrolysis temperatures and Pt/C. (K) Comparative relationship between conductivity, nitrogen content and mesoporous surface area and mass activity of URC materials.

3.2. Plant-based ORR electrocatalysts

Different from animal biomass, plant biomass usually selects specific types of plant biomass with specific structures and enhances electrocatalyst performance with appropriate synthetic strategies. The researchers had done many attempts to convert abundant and inexpensive plant (leaves, fruit, roots or flowers) biomass into ORR efficient ORR catalyst. In this section, we had summarized unique characteristics of biomass, which was important for ORR performance.

Porphyra itself contains proteins and taurine, which can be used as nitrogen, sulfur precursor. On this basis, Zhang et al. obtained nitrogen and sulfur heteroatom doped Fe–N–C material (Fe-NSDC) by mixing and grinding $FeCl_3{\cdot}6H_2O$ with porphyra as precursor and pyrolysis at high temperature (Fig. 5A) [118]. Interestingly, the researcher used ultrasound-assisted strategy to remove taurine contained in porphyra and prepared iron-doped carbon catalyst (Fe-NDC) without sulfur, so as to compare the effect of sulfur and Fe-N_x on improving oxygen reduction activity. Because of the catalysis of Fe, the Fe-NSDC catalyst exhibited a three-dimensional layered sheet-like structure. And the thin-layer sheet-like structures with porous and wavy corrugated structures of Fe-NSDC can provide additional active site and facilitated electron transfer. Fe–N_3|S can be found as Fe-NSDC catalytic active site by XAS analysis. The Fe-NSDC catalyst exhibited ultra-high performance with $E_{1/2}$ up to 0.84 V *vs.* RHE, which was superior to Pt/C catalyst performance (Fig. 5B and C). It was found that the addition of S can adjust the charge distribution of Fe-NSDC catalyst, resulting in excellent ORR

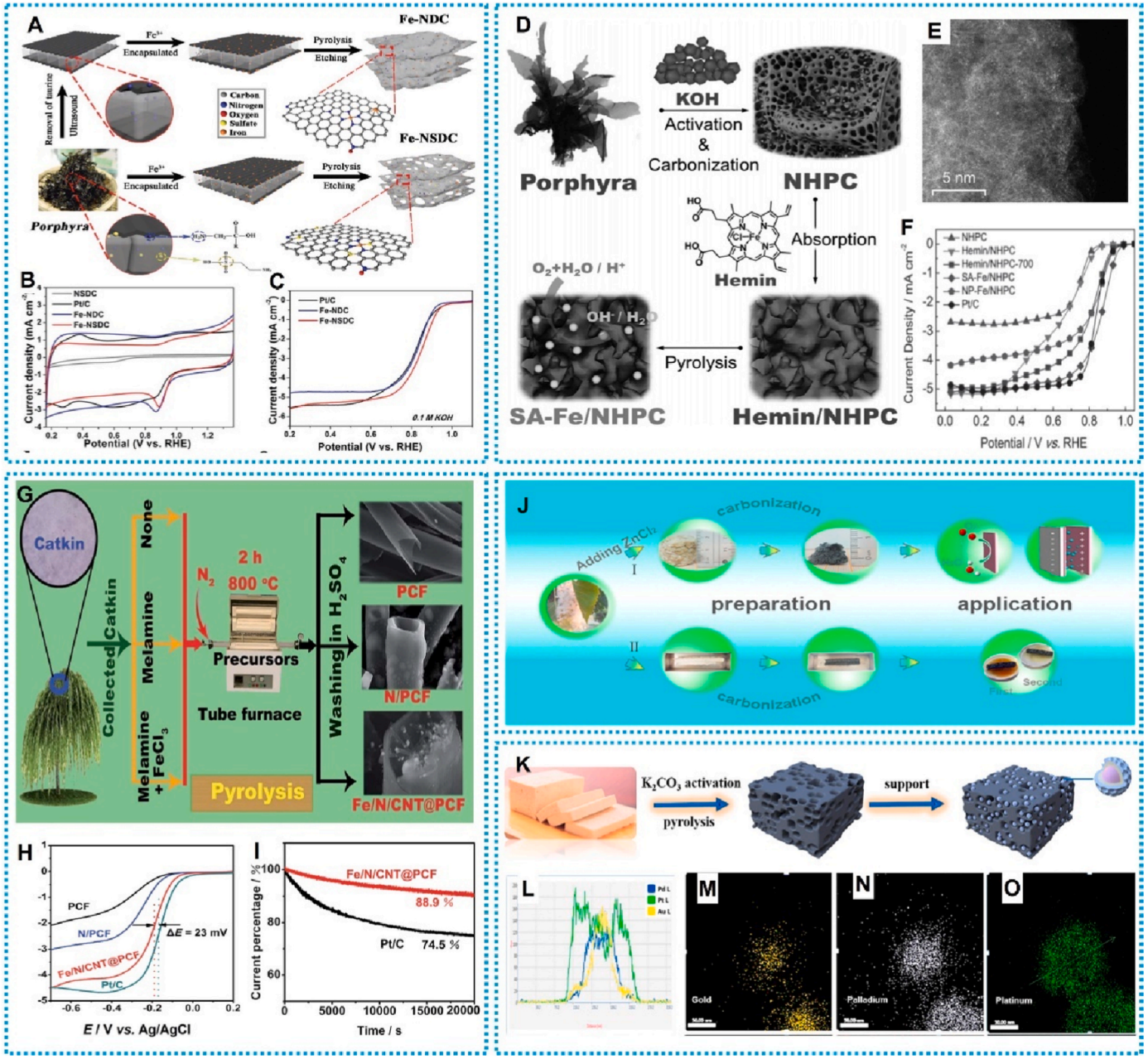

Fig. 5. (A) Schematic procedure to obtain Fe-NSDC with porphyra as precursor [118]. (B) CV curves and (C) LSV curves of Fe-NDC, Fe-NSDC and Pt/C catalyst. (D) Synthesis procedure of SA-Fe/NHPC catalyst [119]. (E) HAADF-STEM of SA-Fe/NHPC catalyst. (F) LSV curves of SA-Fe/NHPC catalyst. (G) Schematic diagram of preparation of Fe/N/CNT@PCFs by direct carbonizing of catkins [120]. (H) LSV curves of Fe/N/CNT@PCF and Pt/C catalyst. (I) The durability tests of Fe/N/CNT@PCF and Pt/C catalyst. (J) The formation process of carbon with high porosity by using catkins as precursor [121]. (K) Synthesis procedure of Au@Pd@Pt-NSC-900 composite [106]. (L) Line-scanning of Au@Pd@Pt core-shell material. (M ~ O) Elemental mapping of Au, Pd and Pt.

activity.

On the basis of the confinement effect of porous carbonaceous material and Fe element, Zhang et al. obtained nitrogen-doped hierarchical porous carbon-supported single-atom Fe (SA-Fe/NHPC) catalyst by rapid pyrolysis of hemin-adsorbed bio-porphyrin carbon (Fig. 5D) [119]. A large number of micropores were embedded in the carbon layer of SA-Fe/NHPC. At the same time, the Fe atoms in micropores are evenly distributed, and there is no obvious aggregation of metal atoms (Fig. 5E). The as-prepared SA-Fe/NHPC catalyst exhibited great ORR activity ($E_{1/2} = 0.87$ V *vs.* RHE) in alkaline media (Fig. 5F), ORR stability ($E_{1/2}$ negative shift by 1 mV after ADT) and methanol tolerance, which were greater than those of Pt/C catalysts.

Catkins contain C, N and other element, which can be used as natural, inexpensive and sustainable precursor and template materials to prepare heteratomic self-doping carbon catalysts. Li et al. synthesized Fe and N co-doped carbon nanotubes@hollow carbon fiber catalysts (Fe/N/CNT@PCFs) by direct carbonization of catkins, melamine, and $FeCl_3{\cdot}6H_2O$ (Fig. 5G) [120]. The addition of melamine to the carbon material as a nitrogen source greatly increased the nitrogen content. Through characterization, it could be found that the presence of Fe element enables the catalytic growth of many carbon nanotubes on the walls of Fe/N/CNT@PCFs. The special structure of Fe/N/CNT@PCFs endowed it with large SSA. In addition, the presence of Fe also promoted the formation of pyridine nitrogen species, which further enhanced the ORR performance. After testing, Fe/N/CNT@PCFs displayed the most positive E_{onset} of 98 mV and $E_{1/2}$ of 194 mV (Fig. 5H). And after 20000 s test, the relative current of Fe/N/CNT@PCF was as high as 88.9% (Fig. 5I). Gao et al. took catkins as precursor and synthesized carbon with high pore volume (1.31 $cm^3\ g^{-1}$) and surface area (1462.5 $m^{-2}\ g^{-1}$) by pyrolysis of $ZnCl_2$ (Fig. 5J) [121]. The catalyst was better than the Pt/C catalyst in ORR activity, long-term durability and methanol resistance.

As a common soy product, beancurd has protein and carbohydrates [122], making itself as a cheap precursor. It can be converted into nitrogen-doped carbon by pyrolysis and other processes. However, the pure carbon materials prepared from direct carbonizing of beancurd have some disadvantages such as little SSA and poor catalytic activity. On this basis, Sun et al. reported a tofu-derived porous carbon (NSC-900) by activation of K_2CO_3 and pyrolysis and then loaded the Au@Pd@Pt core-shell particles onto the NSC-900 to obtain composite

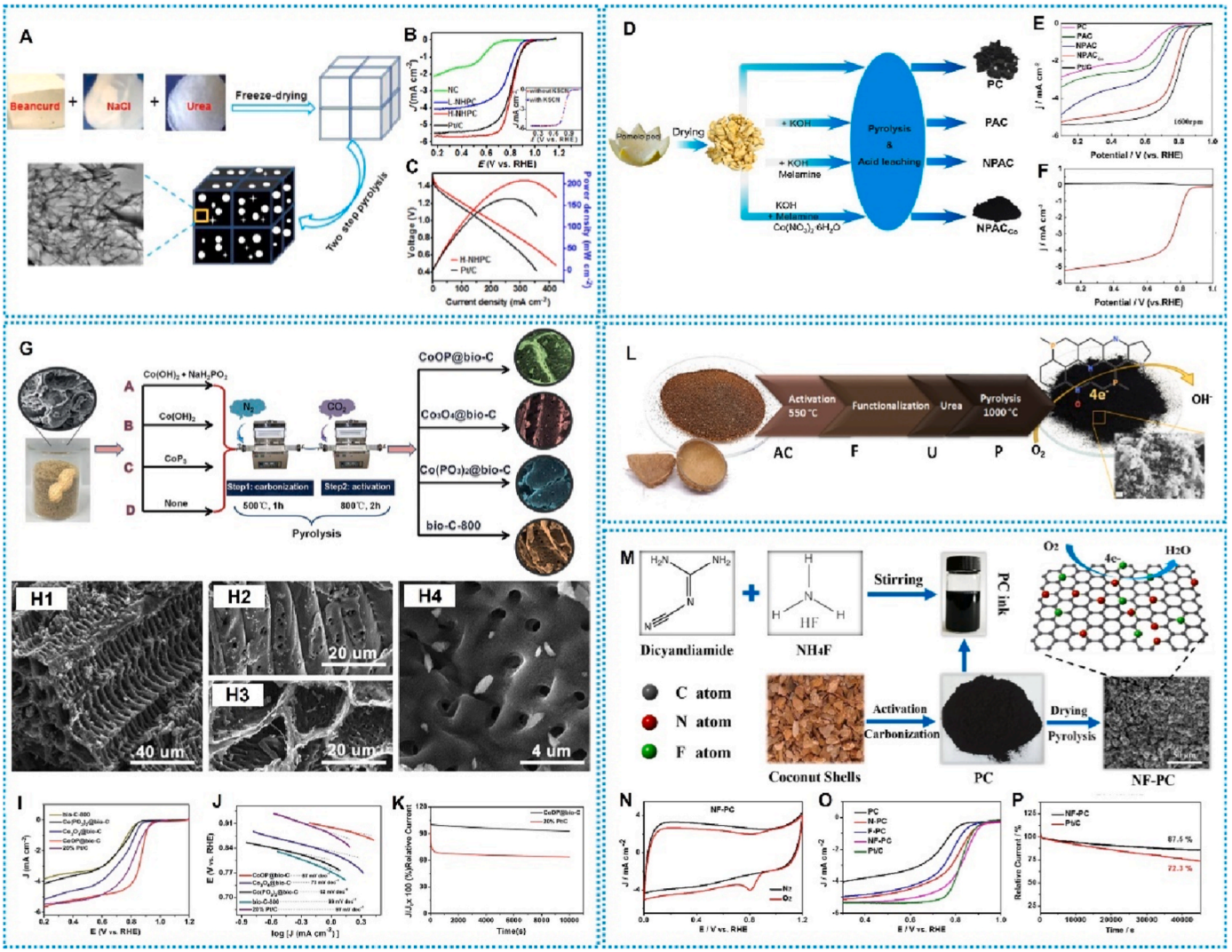

Fig. 6. (A) Schematic procedure to obtain H–NHPC by pyrolysis method using tofu and urea as raw materials and nitrogen sources [123]. (B) LSV curses of H–NHPC and other catalysts. (C) The discharge curves of the H–NHPC-based and Pt/C-based Zn–O_2 battery and corresponding power density. (D) Synthesis procedure of $NPAC_{Co}$ catalyst [125]. (E) LSV curses of $NPAC_{Co}$ and Pt/C catalyst. (F) RDE voltammograms of $NPAC_{Co}$. (G) Synthesis procedure of CoOP@bio-C using peanut shells as precursors [74]. (H1∼H4) SEM of CoOP@bio-C. (I) LSV curses of CoOP@bio-C and other catalysts. (J) Tafel curses of CoOP@bio-C and other catalysts. (K) The i-t chronoamperometry curves of CoOP@bio-C and other catalysts. (L) Schematic diagram of preparation of AC-F-U-P [130]. (M) The formation process of NF-PC [131]. (N) CVs of NF-PC catalyst. (O) LSVs of NF-PC and other catalysts. (P) The i-t chronoamperometry curves of NF-PC and Pt/C catalyst.

material (Fig. 5K–O) [106]. Due to the activation of K_2CO_3, the as-synthesized composite had an ultrahigh SSA (3814 m^2 g^{-1}) and porous structure (2.08 cm^3 g^{-1}). It was noteworthy that the higher SSA promoted mass transfer, which made the Au@Pd@Pt-NSC-900 have higher ORR performance compared to Pt/C. The specific activities and mass activities of the as-synthesized catalyst were 5 and 13 times as high as those of Pt/C catalyst.

A carbon material (H–NHPC) with porous structure (0.689 cm^3 g^{-1}, 988.2 m^2 g^{-1}) was prepared by pyrolysis method using tofu and urea as raw materials and nitrogen sources (Fig. 6A) [123]. Under the action of NaCl, H–NHPC consisted of graphene-like carbon nanosheets that were interconnected to present a 3D hierarchical porous structure. The H–NHPC catalyst showed extreme catalytic activity with a $E_{1/2} = 0.81$ V *vs*. RHE and four-electron selectivity (Fig. 6B). In addition, the application of H–NHPC to zinc-air batteries with high power density and large specific capacity (Fig. 6C). Zhai et al. prepared a novel Co–N–C catalyst by one-step pyrolysis with soymilk as raw material and the addition of cobalt nitrate [124]. Due to the existence of the Co–N–C structure, the catalyst showed ed outstanding ORR activity in alkaline electrolyte.

Nitrogen, cobalt activated biochar ($NPAC_{Co}$) was obtained by high-temperature carbonization method using cobalt nitrate as cobalt source, potassium hydroxide as chemical activator and pomelo peel as precursor (Fig. 6D) [125]. The successful doping of cobalt enhanced the graphitization of carbon and also increased the doping amount of nitrogen. In addition, pyridine nitrogen content was also increased in $NPAC_{Co}$, which was beneficial to improve the ORR activity. For ORR, $NPAC_{Co}$ catalyst exhibited high E_{onset} of 0.87 V *vs*. RHE, high $E_{1/2}$ of 0.78 V *vs*. RHE and low H_2O_2 yield (Fig. 6E and F), comparable to those of Pt/C. The Fe_3C/WC/GC nanocomposites were prepared by a facile carbothermic reduction method derived from pomelo peel [126]. The incorporation of iron can change the amorphous carbon into Fe_3C and contributed to the graphitization of carbon. In addition, during the pyrolysis process, the interaction between iron and tungsten was very close, which could be well dispersed and embedded into the carbonized matrix. After testing, Fe_3C/WC/GC nanocomposites catalyst had high ORR activity and durability in a neutral pH environment. According to DFT calculations, Fe_3C can provide an active site for ORR, and its (001) surface can dissociate the O–O bond to overcome the ORR barrier.

Waste peanut shells can be used as carbon precursors to synthesize porous carbon materials by pyrolysis and other methods. Wu et al. obtained a Co, S co-doped carbon material (CoOP@bio-C) with microporous structure by CO_2 reduction and high-temperature pyrolysis strategy using peanut shells as carbon precursors (Fig. 6G, H1∼H4) [74]. Due to the unique layered 3D open porous structure of CoOP@bio-C materials, the active sites of S and external doping Co_3O_4 and $Co(PO_3)_2$ were increased, which made it have remarkable ORR catalytic activity. The E_{onset} and $E_{1/2}$ of CoOP@bio-C catalyst in 0.1 M KOH solution were 0.91 V *vs*. RHE and 0.81 V *vs*. RHE, respectively, the tafel slope was 57 mV dec^{-1} and the current density lost only 20% after 10 000 s (Fig. 6I–K).

As a natural lignocellulosic material, coconut shell is also suitable for preparing carbon materials with porous structure because of its abundant carbon content, excellent structure and low ash level [87]. Porous carbon materials with SSA of about 800–1500 m^2 g^{-1} were successfully fabricated using raw coconut shell as precursors [127–129]. Borghei et al. used coconut shell residue as carbon precursor, phosphoric acid as activator and urea as nitrogen source, to prepare N, P-doped porous carbon (AC-F-U-P) by chemical activation method (Fig. 6L) [130]. Phosphate can form connections with lignocellulose, thus preventing the shrinkage and collapse of the structure for AC-F-U-P material during high-temperature carbonization. The obtained AC-F-U-P had a large SSA (1216 m^2 g^{-1}) and plenty of mesopores. And the prepared biomass carbon catalyst exhibited excellent long-term stability.

Wang et al. cleverly manufactured N, F co-doped porous carbon (NF-PC) by a economical and environmentally friendly strategy derived from green coconut shell (Fig. 6M) [131]. The microporous structure and the cooperation between N and F element, enabled the NF-PC to exhibit outstanding ORR activity ($E_{onset} = 0.985$ V *vs*. RHE, $E_{1/2} = 0.834$ V *vs*. RHE) and long-term stability (after 45 000 s, the current density of NF-PC catalyst remains 87.5% of the initial current density), even surpassing that of Pt/C catalyst (Fig. 6NQ).

N-doped partly-graphitized carbon (NPGC) was prepared as a cathode ORR catalyst using cornstalks as precursor, which had outstanding ORR performance and high power density of 1122 mW m^{-2} and long-time running durability [132]. Nitrogen, phosphorus, and iron trimeric nanoporous carbon also prepared from corn silk as precursors provided a good foundation for the development of economical, environmentally friendly and high-yield catalysts [133].

3.3. Glucose derivatives

Glucose, a component of cellulose, was used as a precursor for carbon supports of platinum nanoparticle. Yan et al. prepared mesoporous bowl-like carbons (BLCs) derived from glucose and silica spheres as hard template (Fig. 7A) [134]. BLCs had high SSA (1108.3 m^{-2} g^{-1}) and large porosity volume, which were conducive to the uniform dispersion and loading of Pt particles, and significantly enhanced mass transfer process of ORR. CV exhibited that ORR mass current density of the prepared catalyst was 1.6 times as high as that of the Pt/C.

To get rid of the dependence on Pt, Liu et al. fabricated Ag nanoclusters anchored on carbon nanodots (Ag NC/CNs) by a green method using glucose (Fig. 7B). The as-prepared Ag nanoclusters exhibited excellent catalytic performance for ORR, as well as a four-electron transfer process [135]. Wassne et al. obtained carbon spheres by hydrothermal carbonizing glucose and then prepared spherical core-shell composite particles (TaON@CN) by sol-gel deposition of tantalum oxide (Fig. 7C) [136]. The core-shell composite particles consist of a spherical carbon nitride core and a tantalum (oxy)nitride shell. Electrochemical tests showed that the ORR activity of core-shell composite was significantly higher than that of pure tantalum (oxy)nitride.

Titirici et al. used a novel method to fabricate N-doped carbonaceous aerogels based on the hydrothermal carbonization of glucose derivatives [137]. The as prepared aerogel was obtained from carbohydrate-based derivatives and phenolic compounds, with a N doping level of 3–5 wt % and a SSA of 450 m^2 g^{-1}. Later, Titirici and co-workers futher synthesized N-doped porous carbon aerogels using glucose and cellulose as carbon sources, soybean protein as nitrogen sources and pore-forming guide agent [138]. The porosity of the carbon aerogels was enhanced by heat treatment, and the catalysts exhibited good catalytic activity for ORR. The addition of S had a positive effect on ORR performance except N doping after testing. Qiu et al. prepared regular mesoporous and macroporous N–S-CMK-3 catalyst by hard template method using glucose and thiophene as precursors (Fig. 7D) [139]. And the effects of N and S on the ORR performance of N–S-CMK-3 catalyst were studied. The results showed that N–S-CMK-3 catalyst had excellent ORR performance such as 0.92 V *vs*. RHE for E_{onset} (Figs. 7E), 68 mV dec^{-1} for tafel slope, because of the synergy influence of graphite N and thiophene S structure.

Recently, it has been shown that catalytic performance can be enhanced by introducing transition metals into carbon materials rich in nitrogen. Li et al. fabricated Fe, N doped carbon catalysts (3DHP/Fe–N–C-T, T stands for pyrolysis temperature) with high SSA (906.3 m^2 g^{-1}), mesoporous and macroporous structure by high temperature pyrolysis using SiO_2 spheres as sacrificial template, glucose as precursor and dicyandiamide as nitrogen source, respectively (Fig. 7F and G) [140]. The E_{onset} (about 0 V *vs*. Ag/AgCl) and $E_{1/2}$ (−0.15 V *vs*. Ag/AgCl) of 3DHP/Fe–N–C-900 in alkaline medium were comparable to Pt/C catalysts due to cooperation of Fe_3O_4, and N group (Fig. 7H).

Lai et al. fabricated Fe–N/G catalysts by an in-situ self-sacrificial template method to using melamine and glucose as precursors (Fig. 7I) [141]. Under high temperature pyrolysis, Fe/Fe_3C was encapsulated in carbon nanocapsules and then evenly formed on the surface of NG

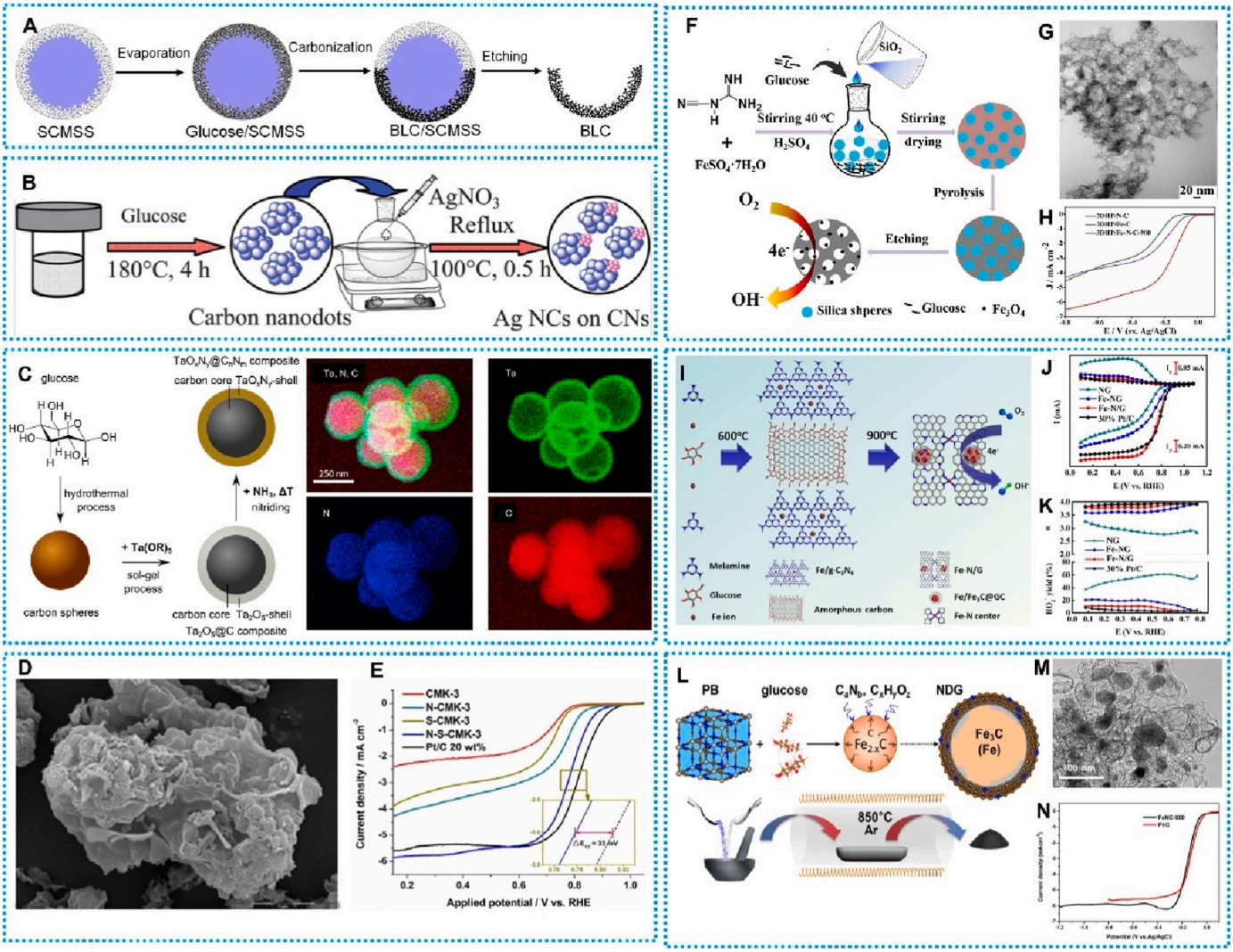

Fig. 7. (A) Schematic procedure to obtain BLCs using glucose as carbon precursor and hard template method [134]. (B) Synthesis procedure of Ag NC/CNs catalyst [135]. (C) The formation process of core-shell TaON@CN and EDS mapping images of TaON@CN [136]. (D) SEM image of N–S-CMK-3 catalyst. (E) LSV curves of N–S-CMK-3 and Pt/C catalyst [139]. (F) Synthesis procedure of 3DHP/Fe–N–C-T [140]. (G) TEM images of 3DHP/Fe–N–C-900. (H) LSV curves of 3DHP/Fe–N–C-900 and other catalysts. (I) Schematic procedure to obtain Fe–N/G [141]. (J) RRDE of Fe–N/G and other catalysts. (K) HO_2^- yield and electron transfer number of the corresponding catalyst. (L) Synthesis procedure of FeNC-850 [142]. (M) TEM of FeNC-850. (N) LSV curves of FeNC-850 and Pt/C.

material with a highly open mesoporous structure. The Fe–N/G catalyst had excellent catalytic activity and four-electron selectivity comparable to those of Pt/C because of its highly active Fe-N_x sites (Fig. 7J and K). Likewise, metal particles can be encapsulated in graphite carbon layers. Yang et al. obtained an Fe–N co-doped catalyst (FeNC-850) through pyrolysis process using glucose and Prussian blue (PB) as precursors (Fig. 7L and M) [142]. During high temperature carbonization, Prussian blue can be decomposed into iron species and iron species catalyzed the growth of graphite layers to form Fe/Fe_3C encapsulation structures. After electrochemical testing, it was found that the prepared FeNC-850 catalyst had excellent ORR performance (Fig. 7N). In addition, when the timing current was carried out in alkaline medium, the current loss was 17.85% after 10000 s, which was less than that of Pt/C catalyst (33.53%), confirming that FeNC-850 catalyst had good long-term stability.

3.4. Starch

Zhao et al. prepared highly active metal-free N-containing carbon nanosheets (NCNs) by one-step pyrolysis method derived from corn-starch and urea [143]. The RDE tests revealed that NCN possessed a four-electron transfer process and exhibited excellent ORR performance and durability, making it an alternative to Pt-based catalysts. Cheng et al. used soluble starch (SS) to encapsulate noble nanoparticles, followed by pyrolysis at low temperature to synthesize ultra-thin carbon layers (UTCL) stabilized Pt catalyst (Pt-UTCL/C) with open frameworks [144]. The special structure of UTCL reduced the loss of ECSA and effectively promoted the ORR mass transfer process. UTCL can tightly fix Pt nanoparticles on the carbon matrix, inhibited the agglomeration and separation of Pt nanoparticles, and slowed down their dissolution growth process. Electrochemical tests indicated that the Pt-UTCL/C catalyst had high stability, which was comparable to Pt/C catalysts. Fe, S-modified N-doped graphene/carbon nanosheets (Fe, S/NGC) were obtained by hydrothermal reaction and high-temperature carbonization with graphene oxide (GO), starch, $FeCl_3$ and KSCN [63]. It was precisely shown that Fe, S/NGC had a highly interpenetrated three-dimensional porous structure which was composed of many interconnected nanoflakes with a thickness of 14 nm. Due to the three-dimensional porosity of Fe, S/NGC-900 and synergistic effect of N, S and Fe elements, the obtained Fe, S/NGC-900 catalysts exhibited positive E_{onset} of 0.95 V *vs.* RHE, high $E_{1/2}$ of 0.83 V *vs.* RHE and good kinetic such as low Tafel slopes of 67 mV dec^{-1}.

3.5. Chitin and chitosan

Chitin can serve as both carbon and nitrogen sources at the same time to obtain self-nitrogen-doped carbon materials due to its rich nitrogen content [145]. Li et al. employed a facile solution-chemical method to extract chitin aerogels with micropores and mesopores from shrimp shells, followed by carbonization to obtain N-doped carbon materials (Chitin-900) (Fig. 8A). The prepared Chitin-900 catalyst had a typical four-electron oxygen reduction path (Fig. 8B). Wu et al. obtained N-doped carbon/graphite C_3N_4 (C-Chitin/g-C_3N_4) catalyst by dissolving and pyrolysis of g-C_3N_4 and chitin at high temperature (Fig. 8C) [146]. The C-chitin/g-C_3N_4 composite exhibited a unique three-dimensional (3D) loofah-like network structure, which enhanced the contact opportunity between the cathode ORR catalyst and the electrolyte, promoted mass transfer, and was beneficial to expose the ORR catalytic active sites. Benefiting from the well-designed porous structure, the C-Chitin/g-C_3N_4 catalyst exhibited obvious ORR activity (Fig. 8D) and excellent methanol resistance, etc.

Titirici et al. obtained nitrogen-doped carbon by a one-pot pyrolysis method using lobster shells and artificial lobster shells which was composed of chitin and $CaCO_3$ particles as precursors, respectively [147]. Due to the relatively uniform distribution of $CaCO_3$ particles in the artificial shrimp shell, chitin-derived carbon had a higher SSA. The chitin-derived catalyst had higher E_{onset} and lower H_2O_2 yield after tests. Activated carbon sheets (ACS) were synthsized by hydrothermal carbonization using chitin as precursor and zinc chloride as activator (Fig. 8E) [148]. Chitin-based carbons had sheet-like morphology and are composed of porous structures. The ACS catalyst exhibited obvious catalytic activity, excellent long-term durability and methanol resistancein alkaline electrolyte, comparable to Pt/C catalysts. (Fig. 8F), Chitosan is a sustainable and inexpensive biomass precursor capable of forming N-active sites in carbon materials. Zhang et al. fabricated metal-free mesoporous N-doped carbon materials by adding different kinds of pore-forming agents and using chitosan as precursor (Fig. 8G and H) [149]. Interestingly, the SSA (1190 m^2/g^{-1}) of N-doped mesoporous biomass carbon (NC-3) increased significantly after adding ferric nitrate as a pore former. The synthesized NC-3 catalyst contained a large amount of pyridine N, indicating that Fe doping can regulate the generation of pyridine N, thereby promoting the four-electron reaction and improving the ORR activity (Fig. 8I and J). Highly graphitized graphene-like N-doped mesoporous carbon (STST, T stands for temperature) by high temperature pyrolysis using $FeCl_3$ as a soft template

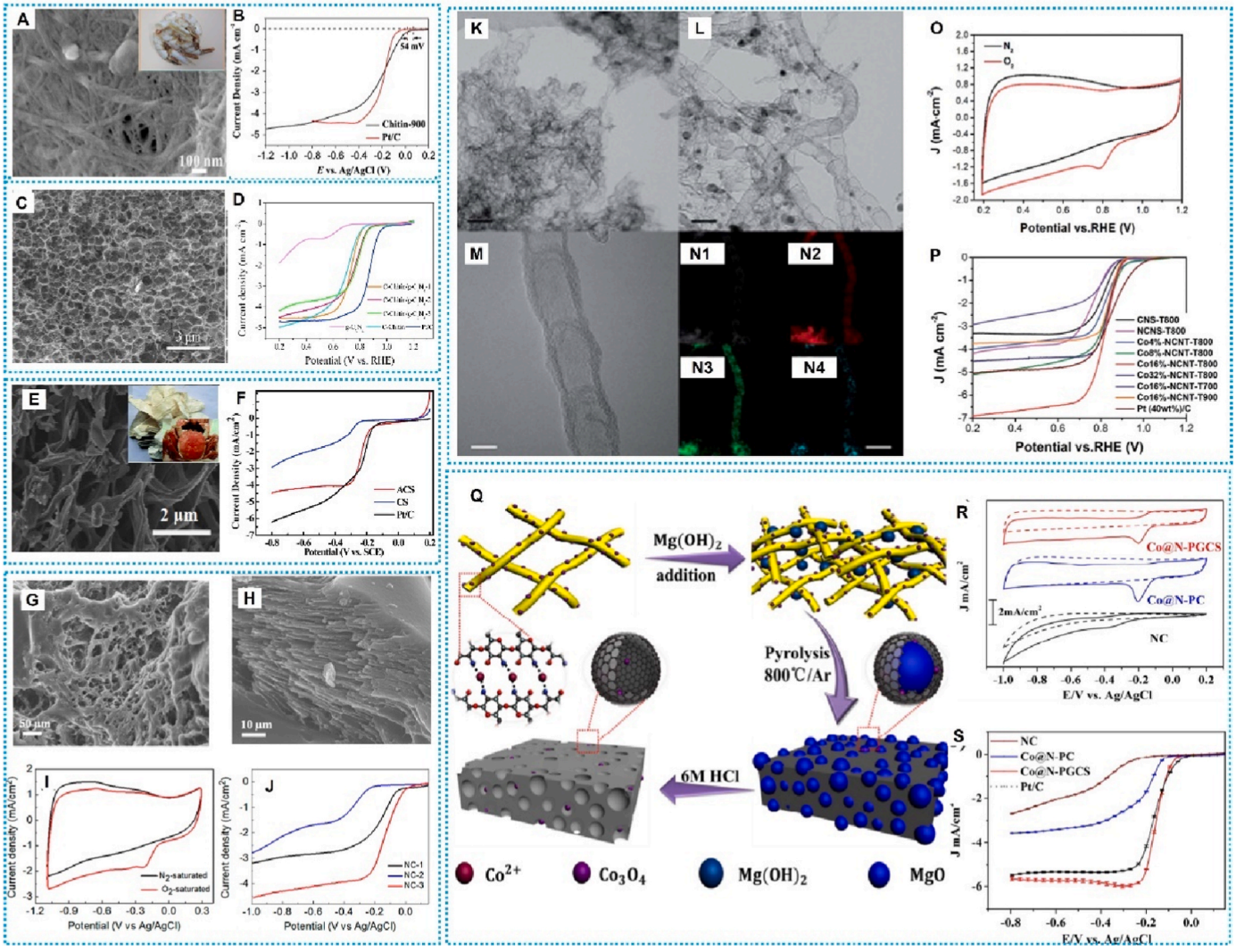

Fig. 8. (A) SEM of Chitin-900 [145]. (B) LSV of Chitin-900 and Pt/C catalyst. (C) SEM of C-chitin/g-C_3N_4 [146]. (D) LSV curves of C-chitin/g-C_3N_4 and other catalysts. (E) SEM image of ACS [148]. (F) LSV curves of ACS and Pt/C catalyst. (G, H) SEM image of NC-3 [149]. (I) CV curves of NC-3 catalyst. (J) LSV curves of NC-3 and Pt/C catalyst. TEM images of (K) nitrogen doped carbon and (L) CoNCNT-T800 [154]. (M) HRTEM image of Co-NCNT-T800. (M) STEM images and (N1~N4) EDS mappings of Co-NCNT-T800. (O) CV curves of Co-NCNT-T800 catalyst. (P) LSV curves of Co-NCNT-T800 and Pt/C catalyst. (Q) Synthesis procedure of Co@N-PGCS [155]. (R) CV and (S) LSVcurves of Co@N-PGCS and corresponding catalysts.

[150]. The carbon material structure and N species can be regulated by tuning the carbonization temperature. STS800 pyrolyzed at 800 °C showed excellent ORR performance due to high graphitization and abundant pyridinic N and graphitic N species. Later, Tong et al. used chitosan as the precursor, triphenylphosphine as the phosphorus source, and $ZnCl_2$ as the activated pore-forming agent to prepare N, P double-doped porous graphite carbon materials by hydrothermal reaction and carbonization [151]. P doping can significantly increase the BET SSA and pore volume of carbon materials and enhance charge delocalization to obtain carbon structures with more defects and edge sites. Compared with the Pt/C, the as-prepared catalyst showed comparable ORR activity ($E_{onset} = -0.014$ V *vs.* AgCl) and better methanol resistance.

Transition metal/carbon ORR catalysts with strong M-N-C bonds exhibit synergistic effects in further improving their ORR performance [152,153]. Zhang et al. used chitosan to obtain cobalt-doped nitrogen-containing carbon nanotube (Co-NCNTs) ORR catalysts through high temperature carbonization pyrolysis and catalyzed by transition metal cobalt (Fig. 8K–N4) [154]. It was found that the doping of cobalt changed the shape of the carbon matrix from nanosheet to nanotube (Fig. 8K and L). The successful synthesis of Co–N–C active sites was crucial for improving the ORR performance of the Co-NCNTs. The $E_{1/2}$ of the Co-NCNT catalyst was 0.839 V *vs.* RHE, which was comparable to that of Pt/C (Fig. 8O and P). Co, N co-doped carbon nanosheets (Co@N-PGCS) were obtained by a facile $Mg(OH)_2$ nanocasting strategy using chitosan as carbon source (Fig. 8Q) [155]. The structure of Co@N-PGCS was mainly mesoporous and had a large BET SSA (1716 m^2 g^{-1}) and pore volume (1.55 cm^3 g^{-1}), thus promoting the diffusion of reactive species. Compared with Pt/C, Co@N-PGCS exhibited excellent activity with −0.075 V *vs.* AgCl for E_{onset} and −0.151 V *vs.* AgCl for $E_{1/2}$ in 0.1 M KOH (Fig. 8R and S).

4. Conclusion and outlook

ORR plays an essential role in the performance of energy conversion storage devices. Therefore, technological progress towards economical, efficient, and sustainable materials is very necessity. The work above showed that biomass from plants, animals, and carbohydrates holded out great prospects as precursors for superior ORR electrocatalysts. Although biomass carbon is versatile, the advantages and disadvantages of each biomass carbon are obvious. Animal biomass carbon can contain elements that are unique to the catalytic activity center, such as iron in pig blood biomass carbon, but it is difficult to have fixed morphological characteristics in animal biomass carbon. Plant biomass carbon can be utilized with the original morphological characteristics of the plant, for example, stem biomass can retain the original tube packing structure, but basically all biomass carbon pore structures are difficult to regulate, and the pore structure is very complex. Glucose derivatives and chitosan-like substances can be made into nanospheres, as well as can be combined with drinking multi-catalytic active centers, but the relationship between their catalytic active centers and heteroatoms in biomass is not clear.

However, the differences between the same organisms growing in different areas make reproducibility difficult. Hence, in order to develop superior catalysts, this issue should be addressed. First, more attention should be paid to the properties of various biomass, and a general reproducible preparation route that is more suitable for different organisms should be designed. Second, standard experimental parameters which are essential to the reproducibility should be well controlled, including the manufacturer and origin. Finally, the general applicability of similar fractions across various biomass should be considered so as to further develop reproducibility. It is believed that a mass of rational preparation process will emerge in the next few years for the manufacture of new sustainable carbon-based materials from biomass resources, and it is hoped that this research will contribute to a wider application of sustainable carbon-based materials.

Data availability

No data was used for the research described in the article.

References

[1] Z. Zhao, M. Li, L. Zhang, L. Dai, Z. Xia, Design principles for heteroatom-doped carbon nanomaterials as highly efficient catalysts for fuel cells and metal-air batteries, Adv. Mater. 27 (43) (2015) 6834–6840, https://doi.org/10.1002/adma.201503211.

[2] N. Han, M. Race, W. Zhang, R. Marotta, C. Zhang, A. Bokhari, J.J. Klemeš, Perovskite and related oxide based electrodes for water splitting, J. Clean. Prod. 318 (2021), https://doi.org/10.1016/j.jclepro.2021.128544.

[3] N. Han, P. Liu, J. Jiang, L. Ai, Z. Shao, S. Liu, Recent advances in nanostructured metal nitrides for water splitting, J. Mater. Chem. 6 (41) (2018) 19912–19933, https://doi.org/10.1039/c8ta06529b.

[4] L. Jiang, F. Liang, Z. Zhang, D. Wu, J. Chai, T. Luo, N. Han, W. Zhang, Y. Rui, B. Tang, A novel cobalt chloride hydrate modified Co-MOF derived carbon microspheres as anode materials for lithium ion batteries, Chem. Eng. J. 433 (2022), https://doi.org/10.1016/j.cej.2021.133568.

[5] Z. Chen, X. Gu, Y. Guo, X. Wang, M. Shao, B. Dong, Z. Kang, A carbon dot-based total green and self-recoverable solid-state electrochemical cell fully utilizing O_2/H_2O redox couple, SusMat 1 (3) (2021) 448–457, https://doi.org/10.1002/sus2.23.

[6] G. Wu, A. Santandreu, W. Kellogg, S. Gupta, O. Ogoke, H. Zhang, H.-L. Wang, L. Dai, Carbon nanocomposite catalysts for oxygen reduction and evolution reactions: from nitrogen doping to transition-metal addition, Nano Energy 29 (2016) 83–110, https://doi.org/10.1016/j.nanoen.2015.12.032.

[7] P. Liu, N. Han, W. Wang, R. Ran, W. Zhou, Z. Shao, High-Quality ruddlesden-popper perovskite film formation for high-performance perovskite solar cells, Adv. Mater. 33 (10) (2021), e2002582, https://doi.org/10.1002/adma.202002582.

[8] J. Niu, R. Shao, M. Liu, Y. Zan, M. Dou, J. Liu, Z. Zhang, Y. Huang, F. Wang, Porous carbons derived from collagen-enriched biomass: tailored design, synthesis, and application in electrochemical energy storage and conversion, Adv. Funct. Mater. 29 (46) (2019), https://doi.org/10.1002/adfm.201905095.

[9] N. Han, X. Guo, J. Cheng, P. Liu, S. Zhang, S. Huang, M.R. Rowles, J. Fransaer, S. Liu, Inhibiting in situ phase transition in Ruddlesden-Popper perovskite via tailoring bond hybridization and its application in oxygen permeation, Matter 4 (5) (2021) 1720–1734, https://doi.org/10.1016/j.matt.2021.02.019.

[10] H. Liu, L. Syama, L. Zhang, C. Lee, C. Liu, Z. Dai, Q. Yan, High-entropy alloys and compounds for electrocatalytic energy conversion applications, SusMat 1 (4) (2021) 482–505, https://doi.org/10.1002/sus2.32.

[11] Y. Wu, Y. Li, J. Gao, Q. Zhang, Recent advances in vacancy engineering of metal-organic frameworks and their derivatives for electrocatalysis, SusMat 1 (1) (2021) 66–87, https://doi.org/10.1002/sus2.3.

[12] J. Wang, L. Ma, J. Xu, Y. Xu, K. Sun, Z. Peng, Oxygen electrochemistry in Li-O_2 batteries probed by in situ surface-enhanced Raman spectroscopy, SusMat 1 (3) (2021) 345–358, https://doi.org/10.1002/sus2.24.

[13] Z. Lei, C.I. Sathish, Y. Liu, A. Karokoti, J. Wang, L. Qiao, A. Vinu, J. Yi, Single metal atoms catalysts—promising candidates for next generation energy storage and conversion devices, EcoMat 4 (3) (2022), https://doi.org/10.1002/eom2.12186.

[14] B. Jing, S. You, Y. Ma, Z. Xing, H. Chen, Y. Dai, C. Zhang, N. Ren, J. Zou, Fe_3Se_4/FeSe heterojunctions in cornstalk-derived N-doped carbon framework enhance charge transfer and cathodic oxygen reduction reaction to boost bio-electricity generation, Appl. Catal. B Environ. 244 (2019) 465–474, https://doi.org/10.1016/j.apcatb.2018.11.074.

[15] B. Dunn, H. Kamath, J.M. Tarascon, Electrical energy storage for the grid: a battery of choices, Science 334 (6058) (2011) 928–935, https://doi.org/10.1126/science.1212741.

[16] J. Yang, X. Wang, B. Li, L. Ma, L. Shi, Y. Xiong, H. Xu, Novel iron/cobalt-containing polypyrrole hydrogel-derived trifunctional electrocatalyst for self-powered overall water splitting, Adv. Funct. Mater. 27 (17) (2017), https://doi.org/10.1002/adfm.201606497.

[17] Y. Liang, Y. Cui, Y. Chao, N. Han, J. Sunarso, P. Liang, X. He, C. Zhang, S. Liu, Exsolution of CoFe(Ru) nanoparticles in Ru-doped $(La_{0.8}Sr_{0.2})_{0.9}Co_{0.1}Fe_{0.8}Ru_{0.1}O_{3-\delta}$ for efficient oxygen evolution reaction, Nano Res. (2022), https://doi.org/10.1007/s12274-022-4328-0.

[18] N. Han, Z. Shen, X. Zhao, R. Chen, V.K. Thakur, Perovskite oxides for oxygen transport: chemistry and material horizons, Sci. Total Environ. 806 (2022), 151213, https://doi.org/10.1016/j.scitotenv.2021.151213.

[19] Y. Liang, D. Ye, N. Han, P. Liang, J. Wang, G. Yang, C. Zhang, X. He, M. Chen, C. Zhang, Nanoporous silver-modified LaCoO3-δ perovskite for oxygen reduction reaction, Electrochim. Acta 391 (2021), https://doi.org/10.1016/j.electacta.2021.138908.

[20] A.I. Douka, H. Yang, L. Huang, S. Zaman, T. Yue, W. Guo, B. You, B.Y. Xia, Transition metal/carbon hybrids for oxygen electrocatalysis in rechargeable zinc-air batteries, EcoMat 3 (1) (2020), https://doi.org/10.1002/eom2.12067.

[21] M. Liu, J. Lee, T.C. Yang, F. Zheng, J. Zhao, C.M. Yang, L.Y.S. Lee, Synergies of Fe single atoms and clusters on N-doped carbon electrocatalyst for pH-universal oxygen reduction, Small Methods 5 (5) (2021), e2001165, https://doi.org/10.1002/smtd.202001165.

[22] N. Zhang, T. Zhou, J. Ge, Y. Lin, Z. Du, C.a. Zhong, W. Wang, Q. Jiao, R. Yuan, Y. Tian, W. Chu, C. Wu, Y. Xie, High-density planar-like Fe2N6 structure catalyzes efficient oxygen reduction, Matter 3 (2) (2020) 509–521, https://doi.org/10.1016/j.matt.2020.06.026.
[23] N. Xu, Y. Zhang, M. Wang, X. Fan, T. Zhang, L. Peng, X.-D. Zhou, J. Qiao, High-performing rechargeable/flexible zinc-air batteries by coordinated hierarchical Bi-metallic electrocatalyst and heterostructure anion exchange membrane, Nano Energy 65 (2019), https://doi.org/10.1016/j.nanoen.2019.104021.
[24] L. Diao, T. Yang, B. Chen, B. Zhang, N. Zhao, C. Shi, E. Liu, L. Ma, C. He, Electronic reconfiguration of Co2P induced by Cu doping enhancing oxygen reduction reaction activity in zinc–air batteries, J. Mater. Chem. 7 (37) (2019) 21232–21243, https://doi.org/10.1039/c9ta07652b.
[25] J. Zhang, Z. Zhao, Z. Xia, L. Dai, A metal-free bifunctional electrocatalyst for oxygen reduction and oxygen evolution reactions, Nat. Nanotechnol. 10 (5) (2015) 444–452, https://doi.org/10.1038/nnano.2015.48.
[26] Z. Xiao, Y. Wu, S. Cao, W. Yan, B. Chen, T. Xing, Z. Li, X. Lu, Y. Chen, K. Wang, J. Jiang, An active site pre-anchoring and post-exposure strategy in $Fe(CN)_6^{4-}$@PPy derived Fe/S/N-doped carbon electrocatalyst for high performance oxygen reduction reaction and zinc-air batteries, Chem. Eng. J. 413 (2021), https://doi.org/10.1016/j.cej.2020.127395.
[27] J. Liang, Y. Xia, X. Liu, F. Huang, J. Liu, S. Li, T. Wang, S. Jiao, R. Cao, J. Han, H. L. Wang, Q. Li, Molybdenum-doped ordered L10-PdZn nanosheets for enhanced oxygen reduction electrocatalysis, SusMat (2022), https://doi.org/10.1002/sus2.65.
[28] B. Huang, Y. Zhao, Iridium-based electrocatalysts toward sustainable energy conversion, EcoMat 4 (2) (2022), https://doi.org/10.1002/eom2.12176.
[29] X. Ao, W. Zhang, Z. Li, J.G. Li, L. Soule, X. Huang, W.H. Chiang, H.M. Chen, C. Wang, M. Liu, X.C. Zeng, Markedly enhanced oxygen reduction activity of single-atom Fe catalysts via integration with Fe nanoclusters, ACS Nano 13 (10) (2019) 11853–11862, https://doi.org/10.1021/acsnano.9b05913.
[30] H.W. Liang, X. Zhuang, S. Bruller, X. Feng, K. Mullen, Hierarchically porous carbons with optimized nitrogen doping as highly active electrocatalysts for oxygen reduction, Nat. Commun. 5 (2014) 4973, https://doi.org/10.1038/ncomms5973.
[31] Y. Cao, W. Zhang, Y. Sun, Y. Jiang, N. Han, J. Zou, W. Si, F. Wang, A. Nunez-Delgado, S. Liu, Highly active iron-nitrogen-boron-carbon bifunctional electrocatalytic platform for hydrogen peroxide sensing and oxygen reduction, Environ. Res. 201 (2021), 111563, https://doi.org/10.1016/j.envres.2021.111563.
[32] W. Zhang, N. Han, J. Luo, X. Han, S. Feng, W. Guo, S. Xie, Z. Zhou, P. Subramanian, K. Wan, J. Arbiol, C. Zhang, S. Liu, M. Xu, X. Zhang, J. Fransaer, Critical role of phosphorus in hollow structures cobalt-based phosphides as bifunctional catalysts for water splitting, Small 18 (4) (2022), e2103561, https://doi.org/10.1002/smll.202103561.
[33] Y. Lei, F. Yang, H. Xie, Y. Lei, X. Liu, Y. Si, H. Wang, Biomass in situ conversion to Fe single atomic sites coupled with Fe2O3 clusters embedded in porous carbons for the oxygen reduction reaction, J. Mater. Chem. 8 (39) (2020) 20629–20636, https://doi.org/10.1039/d0ta06022d.
[34] Q. Wei, X. Yang, G. Zhang, D. Wang, L. Zuin, D. Banham, L. Yang, S. Ye, Y. Wang, M. Mohamedi, S. Sun, An active and robust Si-Fe/N/C catalyst derived from waste reed for oxygen reduction, Appl. Catal. B Environ. 237 (2018) 85–93, https://doi.org/10.1016/j.apcatb.2018.05.046.
[35] L. Liu, X. Zhao, R. Li, H. Su, H. Zhang, Q. Liu, Subnano amorphous Fe-based clusters with high mass activity for efficient electrocatalytic oxygen reduction reaction, ACS Appl. Mater. Interfaces 11 (44) (2019) 41432–41439, https://doi.org/10.1021/acsami.9b15397.
[36] W.-T. Wang, N. Batool, T.-H. Zhang, J. Liu, X.-F. Han, J.-H. Tian, R. Yang, When MOFs meet MXenes: superior ORR performance in both alkaline and acidic solutions, J. Mater. Chem. 9 (7) (2021) 3952–3960, https://doi.org/10.1039/d0ta10811a.
[37] T. Zhang, B. Zhang, Q. Peng, J. Zhou, Z. Sun, Mo_2B_2 MBene-supported single-atom catalysts as bifunctional HER/OER and OER/ORR electrocatalysts, J. Mater. Chem. 9 (1) (2021) 433–441, https://doi.org/10.1039/d0ta08630d.
[38] L. Yang, X. Liu, J. Ding, S. Li, F. Dong, M. Irfan, Y. Li, G. Wang, X. Du, P. Zhang, Chlorella-derived porous heteroatom-doped carbons as robust catalysts for oxygen reduction reaction in direct glucose alkaline fuel cell, Int. J. Hydrogen Energy 44 (5) (2019) 2823–2831, https://doi.org/10.1016/j.ijhydene.2018.12.032.
[39] R. Wang, H. Song, H. Li, H. Wang, X. Mao, S. Ji, Mesoporous nitrogen-doped carbon derived from carp with high electrocatalytic performance for oxygen reduction reaction, J. Power Sources 278 (2015) 213–217, https://doi.org/10.1016/j.jpowsour.2014.12.072.
[40] L. Peng, Z. Fang, Y. Zhu, C. Yan, G. Yu, Holey 2D nanomaterials for electrochemical energy storage, Adv. Energy Mater. 8 (9) (2018), https://doi.org/10.1002/aenm.201702179.
[41] X. Luo, H. Zheng, W. Lai, P. Yuan, S. Li, D. Li, Y.J.E. Chen, E. Materials, Defect engineering of carbons for energy conversion and storage applications, Energy Environ. Mater., https://doi.org/10.1002/eem2.12402.
[42] M. Sevilla, R. Mokaya, Energy storage applications of activated carbons: supercapacitors and hydrogen storage, Energy Environ. Sci. 7 (4) (2014) 1250–1280, https://doi.org/10.1039/c3ee43525c.
[43] H. Liu, X. Liu, W. Li, X. Guo, Y. Wang, G. Wang, D. Zhao, Porous carbon composites for next generation rechargeable lithium batteries, Adv. Energy Mater. 7 (24) (2017), https://doi.org/10.1002/aenm.201700283.
[44] Q. Wei, F. Xiong, S. Tan, L. Huang, E.H. Lan, B. Dunn, L. Mai, Porous one-dimensional nanomaterials: design, fabrication and applications in electrochemical energy storage, Adv. Mater. 29 (20) (2017), https://doi.org/10.1002/adma.201602300.
[45] J. Liang, Y. Jiao, M. Jaroniec, S.Z. Qiao, Sulfur and nitrogen dual-doped mesoporous graphene electrocatalyst for oxygen reduction with synergistically enhanced performance, Angew. Chem. Int. Ed. 51 (46) (2012) 11496–11500, https://doi.org/10.1002/anie.201206720.
[46] K.A. Shah, B.A. Tali, Synthesis of carbon nanotubes by catalytic chemical vapour deposition: a review on carbon sources, catalysts and substrates, Mater. Sci. Semicond. Process. 41 (2016) 67–82, https://doi.org/10.1016/j.mssp.2015.08.013.
[47] J. Zhang, C. Zhang, Y. Zhao, I.S. Amiinu, H. Zhou, X. Liu, Y. Tang, S. Mu, Three dimensional few-layer porous carbon nanosheets towards oxygen reduction, Appl. Catal. B Environ. 211 (2017) 148–156, https://doi.org/10.1016/j.apcatb.2017.04.038.
[48] Z. Zhang, S. Yang, H. Li, Y. Zan, X. Li, Y. Zhu, M. Dou, F. Wang, Sustainable carbonaceous materials derived from biomass as metal-free electrocatalysts, Adv. Mater. 31 (13) (2019), e1805718, https://doi.org/10.1002/adma.201805718.
[49] P. Falkowski, R.J. Scholes, E. Boyle, J. Canadell, D. Canfield, J. Elser, N. Gruber, K. Hibbard, P. Hogberg, S. Linder, F.T. Mackenzie, B. Moore 3rd, T. Pedersen, Y. Rosenthal, S. Seitzinger, V. Smetacek, W. Steffen, The global carbon cycle: a test of our knowledge of earth as a system, Science 290 (5490) (2000) 291–296, https://doi.org/10.1126/science.290.5490.291.
[50] M. Borghei, J. Lehtonen, L. Liu, O.J. Rojas, Advanced biomass-derived electrocatalysts for the oxygen reduction reaction, Adv. Mater. 30 (24) (2018), e1703691, https://doi.org/10.1002/adma.201703691.
[51] J. Zhang, Q. Li, C. Zhang, L. Mai, M. Pan, S. Mu, A N-self-doped carbon catalyst derived from pig blood for oxygen reduction with high activity and stability, Electrochim. Acta 160 (2015) 139–144, https://doi.org/10.1016/j.electacta.2015.01.200.
[52] Y. Fang, H. Wang, H. Yu, F. Peng, From chicken feather to nitrogen and sulfur co-doped large surface bio-carbon flocs: an efficient electrocatalyst for oxygen reduction reaction, Electrochim. Acta 213 (2016) 273–282, https://doi.org/10.1016/j.electacta.2016.07.121.
[53] R. Sharma, K.K. Kar, Effects of surface roughness and N-content on oxygen reduction reaction activity for the carbon-based catalyst derived from poultry featherfiber, Electrochim. Acta 191 (2016) 876–886, https://doi.org/10.1016/j.electacta.2016.01.166.
[54] K.R. Saravanan, V. Mullaivananathan, N. Kalaiselvi, Dual hetero atom containing bio-carbon: multifunctional electrode material for high performance sodium-ion batteries and oxygen reduction reaction, Electrochim. Acta 176 (2015) 670–678, https://doi.org/10.1016/j.electacta.2015.06.116.
[55] C. Zhao, G. Liu, N. Sun, X. Zhang, G. Wang, Y. Zhang, H. Zhang, H. Zhao, Biomass-derived N-doped porous carbon as electrode materials for Zn-air battery powered capacitive deionization, Chem. Eng. J. 334 (2018) 1270–1280, https://doi.org/10.1016/j.cej.2017.11.069.
[56] B. Li, D. Geng, X.S. Lee, X. Ge, J. Chai, Z. Wang, J. Zhang, Z. Liu, T.S. Hor, Y. Zong, Eggplant-derived microporous carbon sheets: towards mass production of efficient bifunctional oxygen electrocatalysts at low cost for rechargeable Zn-air batteries, Chem. Commun. 51 (42) (2015) 8841–8844, https://doi.org/10.1039/c5cc01999k.
[57] Y. Hao, X. Zhang, Q. Yang, K. Chen, J. Guo, D. Zhou, L. Feng, Z. Slanina, Highly porous defective carbons derived from seaweed biomass as efficient electrocatalysts for oxygen reduction in both alkaline and acidic media, Carbon 137 (2018) 93–103, https://doi.org/10.1016/j.carbon.2018.05.007.
[58] H. Zhang, Y. Wang, D. Wang, Y. Li, X. Liu, P. Liu, H. Yang, T. An, Z. Tang, H.J. S. Zhao, Hydrothermal transformation of dried grass into graphitic carbon-based high performance electrocatalyst for oxygen reduction reaction, Small 10 (16) (2014) 3371–3378, https://doi.org/10.1002/smll.201400781.
[59] D. Yang, X. Liu, W. Zhao, Q. Yan, F. Song, T. Wang, Y. Dai, X. Wan, C. Zhou, Y. Yang, A survey of recent progress on novel catalytic materials with precise crystalline structures for oxidation/hydrogenation of key biomass platform chemicals, EcoMat 3 (6) (2021), https://doi.org/10.1002/eom2.12159.
[60] M. Longhi, S. Marzorati, S. Checchia, B. Sacchi, N. Santo, C. Zaffino, M. Scavini, Sugar-based catalysts for oxygen reduction reaction. Effects of the functionalization of the nitrogen precursors on the electrocatalytic activity, Electrochim. Acta 222 (2016) 781–792, https://doi.org/10.1016/j.electacta.2016.11.036.
[61] Z. Wang, F. Zhang, C. Jin, Y. Luo, J. Sui, H. Gong, R. Yang, La2O3-NCNTs hybrids in-situ derived from $LaNi_{0.9}Fe_{0.1}O_3$-C composites as novel robust bifunctional oxygen electrocatalysts, Carbon 115 (2017) 261–270, https://doi.org/10.1016/j.carbon.2017.01.016.
[62] D. Xu, C. Mu, B. Wang, J. Xiang, W. Ruan, F. Wen, X. Du, Z. Liu, Y. Tian, Fabrication of multifunctional carbon encapsulated Ni@NiO nanocomposites for oxygen reduction, oxygen evolution and lithium-ion battery anode materials, Sci. China Mater. 60 (10) (2017) 947–954, https://doi.org/10.1007/s40843-017-9094-5.
[63] B. Men, Y. Sun, J. Liu, Y. Tang, Y. Chen, P. Wan, J. Pan, Synergistically enhanced electrocatalytic activity of sandwich-like N-doped graphene/carbon nanosheets decorated by Fe and S for oxygen reduction reaction, ACS Appl. Mater. Interfaces 8 (30) (2016) 19533–19541, https://doi.org/10.1021/acsami.6b06329.
[64] A.M. Salaberria, S.C. Fernandes, R.H. Diaz, J. Labidi, Processing of alpha-chitin nanofibers by dynamic high pressure homogenization: characterization and antifungal activity against A. Niger, Carbohydr. Polym. 116 (2015) 286–291, https://doi.org/10.1016/j.carbpol.2014.04.047.

[65] C.O. Tuck, E. Pérez, I.T. Horváth, et al., Valorization of biomass: deriving more value from waste, Science 337 (6095) (2012) 695–699, https://doi.org/10.1126/science.1218930.
[66] V. Dhyani, T. Bhaskar, A comprehensive review on the pyrolysis of lignocellulosic biomass, Renew. Energy 129 (2018) 695–716, https://doi.org/10.1016/j.renene.2017.04.035.
[67] A. Corma, O. de la Torre, M. Renz, N. Villandier, Production of high-quality diesel from biomass waste products, Angew. Chem. Int. Ed. 50 (10) (2011) 2375–2378, https://doi.org/10.1002/anie.201007508.
[68] G. Zhang, X. Liu, L. Wang, H. Fu, Recent advances of biomass derived carbon-based materials for efficient electrochemical energy devices, J. Mater. Chem. 10 (17) (2022) 9277–9307, https://doi.org/10.1039/d2ta01442d.
[69] K. Wang, M. Xu, Z. Gu, P. Ahrenkiel, J. Lee, W. Gibbons, J. Croat, Q. Fan, Pyrrole modified biomass derived hierarchical porous carbon as high performance symmetrical supercapacitor electrodes, Int. J. Hydrogen Energy 41 (30) (2016) 13109–13115, https://doi.org/10.1016/j.ijhydene.2016.05.090.
[70] H. Liu, Y. Cao, F. Wang, W. Zhang, Y. Huang, Pig bone derived hierarchical porous carbon-supported platinum nanoparticles with superior electrocatalytic activity towards oxygen reduction reaction, Electroanalysis 26 (8) (2014) 1831–1839, https://doi.org/10.1002/elan.201400180.
[71] Z. Liu, Z. Li, S. Tian, M. Wang, H. Sun, S. Liang, Z. Chang, G. Lu, Conversion of peanut biomass into electrocatalysts with vitamin B12 for oxygen reduction reaction in Zn-air battery, Int. J. Hydrogen Energy 44 (23) (2019) 11788–11796, https://doi.org/10.1016/j.ijhydene.2019.03.055.
[72] L. Han, X. Cui, Y. Liu, G. Han, X. Wu, C. Xu, B. Li, Nitrogen and phosphorus modification to enhance the catalytic activity of biomass-derived carbon toward the oxygen reduction reaction, Sustain. Energy Fuels 4 (6) (2020) 2707–2717, https://doi.org/10.1039/c9se00985j.
[73] J. Hou, K. Jiang, M. Tahir, X. Wu, F. Idrees, M. Shen, C. Cao, Tunable porous structure of carbon nanosheets derived from puffed rice for high energy density supercapacitors, J. Power Sources 371 (2017) 148–155, https://doi.org/10.1016/j.jpowsour.2017.10.045.
[74] Y. Wu, Y. Chen, H. Wang, C. Wang, A. Wang, S. Zhao, X. Li, D. Sun, J. Jiang, Efficient ORR electrocatalytic activity of peanut shell-based graphitic carbon microstructures, J. Mater. Chem. 6 (25) (2018) 12018–12028, https://doi.org/10.1039/c8ta02839g.
[75] S.S. Sekhon, J.-S. Park, Biomass-derived N-doped porous carbon nanosheets for energy technologies, Chem. Eng. J. 425 (2021), https://doi.org/10.1016/j.cej.2021.129017.
[76] X. Peng, L. Zhang, Z. Chen, L. Zhong, D. Zhao, X. Chi, X. Zhao, L. Li, X. Lu, K. Leng, C. Liu, W. Liu, W. Tang, K.P. Loh, Hierarchically porous carbon plates derived from wood as bifunctional ORR/OER electrodes, Adv. Mater. 31 (16) (2019), e1900341, https://doi.org/10.1002/adma.201900341.
[77] T.A. Khan, A.S. Saud, S.S. Jamari, M.H.A. Rahim, J.-W. Park, H.-J. Kim, Hydrothermal carbonization of lignocellulosic biomass for carbon rich material preparation: a review, Biomass Bioenergy 130 (2019), https://doi.org/10.1016/j.biombioe.2019.105384.
[78] K.Y. Park, K. Lee, D. Kim, Characterized hydrochar of algal biomass for producing solid fuel through hydrothermal carbonization, Bioresour. Technol. 258 (2018) 119–124, https://doi.org/10.1016/j.biortech.2018.03.003.
[79] X. Zhang, B. Gao, S. Zhao, P. Wu, L. Han, X. Liu, Optimization of a "coal-like" pelletization technique based on the sustainable biomass fuel of hydrothermal carbonization of wheat straw, J. Clean. Prod. 242 (2020), https://doi.org/10.1016/j.jclepro.2019.118426.
[80] X. Zhang, R. Liu, Y. Zang, G. Liu, S. Liu, G. Wang, Y. Zhang, H. Zhang, H. Zhao, Shrimp-shell derived carbon nanodots as precursors to fabricate Fe,N-doped porous graphitic carbon electrocatalysts for efficient oxygen reduction in zinc–air batteries, Inorg. Chem. Front. 3 (7) (2016) 910–918, https://doi.org/10.1039/c6qi00059b.
[81] S. Gao, Y. Chen, H. Fan, X. Wei, C. Hu, L. Wang, L. Qu, A green one-arrow-two-hawks strategy for nitrogen-doped carbon dots as fluorescent ink and oxygen reduction electrocatalysts, J. Mater. Chem. 2 (18) (2014), https://doi.org/10.1039/c3ta15443b.
[82] C. Chen, D. Yu, G. Zhao, B. Du, W. Tang, L. Sun, Y. Sun, F. Besenbacher, M. Yu, Three-dimensional scaffolding framework of porous carbon nanosheets derived from plant wastes for high-performance supercapacitors, Nano Energy 27 (2016) 377–389, https://doi.org/10.1016/j.nanoen.2016.07.020.
[83] Y. Li, G. Wang, T. Wei, Z. Fan, P. Yan, Nitrogen and sulfur co-doped porous carbon nanosheets derived from willow catkin for supercapacitors, Nano Energy 19 (2016) 165–175, https://doi.org/10.1016/j.nanoen.2015.10.038.
[84] Q. Niu, K. Gao, Q. Tang, L. Wang, L. Han, H. Fang, Y. Zhang, S. Wang, L. Wang, Large-size graphene-like porous carbon nanosheets with controllable N-doped surface derived from sugarcane bagasse pith/chitosan for high performance supercapacitors, Carbon 123 (2017) 290–298, https://doi.org/10.1016/j.carbon.2017.07.078.
[85] J. Mu, Q. Li, X. Kong, X. Wu, J. Sunarso, Y. Zhao, J. Zhou, S. Zhuo, Characterization of hierarchical porous carbons made from bean curd via K_2CO_3 activation as a supercapacitor electrode, Chemelectrochem 6 (15) (2019) 4022–4030, https://doi.org/10.1002/celc.201900962.
[86] R.G. Pereira, C.M. Veloso, N.M. da Silva, L.F. de Sousa, R.C.F. Bonomo, A.O. de Souza, M.O.d.G. Souza, R.d.C.I. Fontan, Preparation of activated carbons from cocoa shells and siriguela seeds using H_3PO_4 and $ZnCl_2$ as activating agents for BSA and α-lactalbumin adsorption, Fuel Process. Technol. 126 (2014) 476–486, https://doi.org/10.1016/j.fuproc.2014.06.001.
[87] J. Mi, X.-R. Wang, R.-J. Fan, W.-H. Qu, W.-C. Li, Coconut-shell-based porous carbons with a tunable micro/mesopore ratio for high-performance supercapacitors, Energy Fuel. 26 (8) (2012) 5321–5329, https://doi.org/10.1021/ef3009234.
[88] Z. Xu, J. Ma, M. Shi, Y. Xie, C. Feng, Biomass based iron and nitrogen co-doped 3D porous carbon as an efficient oxygen reduction catalyst, J. Colloid Interface Sci. 523 (2018) 144–150, https://doi.org/10.1016/j.jcis.2018.03.092.
[89] Z. Zhang, X. Gao, M. Dou, J. Ji, F. Wang, Fe–Nxmoiety-modified hierarchically porous carbons derived from porphyra for highly effective oxygen reduction reaction, J. Mater. Chem. 5 (4) (2017) 1526–1532, https://doi.org/10.1039/c6ta09124e.
[90] J. Wang, S. Yang, W. Song, J. Zhao, Z. Lu, Q. Zhai, L. Jiang, High-efficiency synthesis of Co, N-doped carbon nanocages by ball milling-hard template method as an active catalyst for oxygen reduction reaction, Int. J. Hydrogen Energy 45 (11) (2020) 6318–6327, https://doi.org/10.1016/j.ijhydene.2019.12.101.
[91] X. Li, B.Y. Guan, S. Gao, X.W. Lou, A general dual-templating approach to biomass-derived hierarchically porous heteroatom-doped carbon materials for enhanced electrocatalytic oxygen reduction, Energy Environ. Sci. 12 (2) (2019) 648–655, https://doi.org/10.1039/c8ee02779j.
[92] H. Quan, X. Fan, W. Wang, W. Gao, Y. Dong, D. Chen, Hierarchically porous carbon derived from biomass: effect of mesopore and heteroatom-doping on electrochemical performance, Appl. Surf. Sci. 460 (2018) 8–16, https://doi.org/10.1016/j.apsusc.2018.01.202.
[93] F. Liu, H. Peng, X. Qiao, Z. Fu, P. Huang, S. Liao, High-performance doped carbon electrocatalyst derived from soybean biomass and promoted by zinc chloride, Int. J. Hydrogen Energy 39 (19) (2014) 10128–10134, https://doi.org/10.1016/j.ijhydene.2014.04.176.
[94] C. Hu, J. Liu, J. Wang, W. She, J. Xiao, J. Xi, Z. Bai, S. Wang, Coordination-assisted polymerization of mesoporous cobalt sulfide/heteroatom (N, S)-doped double-layered carbon tubes as an efficient bifunctional oxygen electrocatalyst, ACS Appl. Mater. Interfaces 10 (39) (2018) 33124–33134, https://doi.org/10.1021/acsami.8b07343.
[95] T. Feng, H. Qin, M. Zhang, Co@C nanoparticle embedded hierarchically porous N-doped hollow carbon for efficient oxygen reduction, Chem. Eur J. 24 (40) (2018) 10178–10185, https://doi.org/10.1002/chem.201801442.
[96] H. Zhou, D. He, A.I. Saana, J. Yang, Z. Wang, J. Zhang, Q. Liang, S. Yuan, J. Zhu, S. Mu, Mesoporous-silica induced doped carbon nanotube growth from metal-organic frameworks, Nanoscale 10 (13) (2018) 6147–6154, https://doi.org/10.1039/C8NR00137E.
[97] L. Lv, D. Zha, Y. Ruan, Z. Li, X. Ao, J. Zheng, J. Jiang, H.M. Chen, W.H. Chiang, J. Chen, C. Wang, A universal method to engineer metal oxide-metal-carbon interface for highly efficient oxygen reduction, ACS Nano 12 (3) (2018) 3042–3051, https://doi.org/10.1021/acsnano.8b01056.
[98] T. Feng, M.J.C.C. Zhang, A mixed-ion strategy to construct CNT-decorated Co/N-doped hollow carbon for enhanced oxygen reduction, Chem. Commun. 54 (82) (2018) 11570–11573, https://doi.org/10.1039/C8CC05959D.
[99] L. Osmieri, R. Escudero-Cid, M. Armandi, A.H.A. Monteverde Videla, J.L. García Fierro, P. Ocón, S. Specchia, Fe-N/C catalysts for oxygen reduction reaction supported on different carbonaceous materials. Performance in acidic and alkaline direct alcohol fuel cells, Appl. Catal. B Environ. 205 (2017) 637–653, https://doi.org/10.1016/j.apcatb.2017.01.003.
[100] X. Jin, Y. Jiang, Q. Hu, S. Zhang, Q. Jiang, L. Chen, L. Xu, Y. Xie, J. Huang, Highly efficient electrocatalysts with CoO/CoFe2O4 composites embedded within N-doped porous carbon materials prepared by hard-template method for oxygen reduction reaction, RSC Adv. 7 (89) (2017) 56375–56381, https://doi.org/10.1039/c7ra09517a.
[101] R. Liu, H. Zhang, S. Liu, X. Zhang, T. Wu, X. Ge, Y. Zang, H. Zhao, G. Wang, Shrimp-shell derived carbon nanodots as carbon and nitrogen sources to fabricate three-dimensional N-doped porous carbon electrocatalysts for the oxygen reduction reaction, Phys. Chem. Chem. Phys. 18 (5) (2016) 4095–4101, https://doi.org/10.1039/c5cp06970j.
[102] R.-L. Liu, W.-J. Ji, T. He, Z.-Q. Zhang, J. Zhang, F.-Q. Dang, Fabrication of nitrogen-doped hierarchically porous carbons through a hybrid dual-template route for CO_2 capture and haemoperfusion, Carbon 76 (2014) 84–95, https://doi.org/10.1016/j.carbon.2014.04.052.
[103] H. Yang, H. Li, H. Wang, R. Wang, A wasted material, duck blood, as a precursor of non-precious catalyst for the oxygen reduction reaction, Fuel Cell. 15 (1) (2015) 214–220, https://doi.org/10.1002/fuce.201400105.
[104] J. Maruyama, J. Okamura, K. Miyazaki, et al., Two-step carbonization as a method of enhancing catalytic properties of hemoglobin at the fuel cell cathode, J. Phys. Chem. C 111 (18) (2007) 6597–6600, https://doi.org/10.1021/jp071451+.
[105] N. Daems, X. Sheng, I.F.J. Vankelecom, et al., Metal-free doped carbon materials as electrocatalysts for the oxygen reduction reaction, J. Mater. Chem. 2 (12) (2014) 4085–4110, https://doi.org/10.1039/C3TA14043A.
[106] Y. Sun, W. Zhang, Q. Wang, N. Han, A. Nunez-Delgado, Y. Cao, W. Si, F. Wang, S. Liu, Biomass-derived N,S co-doped 3D multichannel carbon supported Au@Pd@Pt catalysts for oxygen reduction, Environ. Res. 202 (2021), 111684, https://doi.org/10.1016/j.envres.2021.111684.
[107] C. Guo, W. Liao, Z. Li, C. Chen, Exploration of the catalytically active site structures of animal biomass-modified on cheap carbon nanospheres for oxygen reduction reaction with high activity, stability and methanol-tolerant performance in alkaline medium, Carbon 85 (2015) 279–288, https://doi.org/10.1016/j.carbon.2015.01.007.
[108] J. Guan, Z. Zhang, J. Ji, M. Dou, F. Wang, Hydrothermal synthesis of highly dispersed Co_3O_4 nanoparticles on biomass-derived nitrogen-doped hierarchically porous carbon networks as an efficient bifunctional electrocatalyst for oxygen

reduction and evolution reactions, ACS Appl. Mater. Interfaces 9 (36) (2017) 30662–30669, https://doi.org/10.1021/acsami.7b08533.
[109] C. Guo, R. Hu, W. Liao, Z. Li, L. Sun, D. Shi, Y. Li, C. Chen, Protein-enriched fish "biowaste" converted to three-dimensional porous carbon nano-network for advanced oxygen reduction electrocatalysis, Electrochim. Acta 236 (2017) 228–238, https://doi.org/10.1016/j.electacta.2017.03.169.
[110] H. Wang, K. Wang, H. Song, H. Li, S. Ji, Z. Wang, S. Li, R. Wang, N-doped porous carbon material made from fish-bones and its highly electrocatalytic performance in the oxygen reduction reaction, RSC Adv. 5 (60) (2015) 48965–48970, https://doi.org/10.1039/c5ra09144f.
[111] Z. Zhang, J. Sun, F. Wang, L. Dai, Efficient oxygen reduction reaction (ORR) catalysts based on single iron atoms dispersed on a hierarchically structured porous carbon framework, Angew. Chem. Int. Ed. 57 (29) (2018) 9038–9043, https://doi.org/10.1002/anie.201804958.
[112] H. Wu, J. Geng, H. Ge, Z. Guo, Y. Wang, G. Zheng, Egg-derived mesoporous carbon microspheres as bifunctional oxygen evolution and oxygen reduction electrocatalysts, Adv. Energy Mater. 6 (20) (2016), 1600794, https://doi.org/10.1002/aenm.201600794.
[113] J. Zhang, S. Wu, X. Chen, M. Pan, S. Mu, Egg derived nitrogen-self-doped carbon/carbon nanotube hybrids as noble-metal-free catalysts for oxygen reduction, J. Power Sources 271 (2014) 522–529, https://doi.org/10.1016/j.jpowsour.2014.08.038.
[114] F. Xian, L. Gao, Z. Zhang, H. Zhang, S. Dong, G. Cui, N, P dual-doped multi-wrinkled nanosheets prepared from the egg crude lecithin as the efficient metal-free electrocatalyst for oxygen reduction reaction, Appl. Surf. Sci. 476 (2019) 76–83, https://doi.org/10.1016/j.apsusc.2018.12.293.
[115] R.C. Clay, K. Cook, J.I. Routh, Studies in the composition of human hair, J. Am. Chem. Soc. 62 (10) (1940) 2709–2710, https://doi.org/10.1021/ja01867a030.
[116] N.K. Chaudhari, M.Y. Song, J.S. Yu, Transforming hair into heteroatom-doped carbon with high surface area, Small 10 (13) (2014) 2625–2636, https://doi.org/10.1002/smll.201303831.
[117] N.K. Chaudhari, M.Y. Song, J.S. Yu, Heteroatom-doped highly porous carbon from human urine, Sci. Rep. 4 (2014) 5221, https://doi.org/10.1038/srep05221.
[118] J. Zhang, M. Zhang, Y. Zeng, J. Chen, L. Qiu, H. Zhou, C. Sun, Y. Yu, C. Zhu, Z. Zhu, Single Fe atom on hierarchically porous S, N-codoped nanocarbon derived from porphyra enable boosted oxygen catalysis for rechargeable Zn-air batteries, Small 15 (24) (2019), e1900307, https://doi.org/10.1002/smll.201900307.
[119] Z. Zhang, X. Gao, M. Dou, J. Ji, F. Wang, Biomass derived N-doped porous carbon supported single Fe atoms as superior electrocatalysts for oxygen reduction, Small 13 (22) (2017), https://doi.org/10.1002/smll.201604290.
[120] M. Li, Y. Xiong, X. Liu, C. Han, Y. Zhang, X. Bo, L. Guo, Iron and nitrogen co-doped carbon nanotube@hollow carbon fibers derived from plant biomass as efficient catalysts for the oxygen reduction reaction, J. Mater. Chem. 3 (18) (2015) 9658–9667, https://doi.org/10.1039/c5ta00958h.
[121] S. Gao, X. Li, L. Li, X. Wei, A versatile biomass derived carbon material for oxygen reduction reaction, supercapacitors and oil/water separation, Nano Energy 33 (2017) 334–342, https://doi.org/10.1016/j.nanoen.2017.01.045.
[122] Q. Zhang, C. Wang, B. Li, L. Li, D. Lin, H. Chen, Y. Liu, S. Li, W. Qin, J. Liu, W. Liu, Yang, Research progress in tofu processing: from raw materials to processing conditions, Crit. Rev. Food Sci. Nutr. 58 (9) (2018) 1448–1467, https://doi.org/10.1080/10408398.2016.1263823.
[123] H. Zheng, Y. Zhang, J. Long, R. Li, X. Gou, Nitrogen-doped porous carbon material derived from biomass of beancurd as an efficient electrocatalyst for oxygen reduction and Zn-air fuel cell, J. Electrochem. Soc. 167 (8) (2020), https://doi.org/10.1149/1945-7111/ab907f.
[124] Y. Zhai, C. Zhu, E. Wang, S. Dong, Energetic carbon-based hybrids: green and facile synthesis from soy milk and extraordinary electrocatalytic activity towards ORR, Nanoscale 6 (5) (2014) 2964–2970, https://doi.org/10.1039/c3nr05357a.
[125] M. Zhang, X. Jin, L. Wang, M. Sun, Y. Tang, Y. Chen, Y. Sun, X. Yang, P. Wan, Improving biomass-derived carbon by activation with nitrogen and cobalt for supercapacitors and oxygen reduction reaction, Appl. Surf. Sci. 411 (2017) 251–260, https://doi.org/10.1016/j.apsusc.2017.03.097.
[126] M. Ma, S. You, W. Wang, G. Liu, D. Qi, X. Chen, J. Qu, N. Ren, Biomass-derived porous Fe_3C/tungsten carbide/graphitic carbon nanocomposite for efficient electrocatalysis of oxygen reduction, ACS Appl. Mater. Interfaces 8 (47) (2016) 32307–32316, https://doi.org/10.1021/acsami.6b10804.
[127] W. Li, K. Yang, J. Peng, L. Zhang, S. Guo, H. Xia, Effects of carbonization temperatures on characteristics of porosity in coconut shell chars and activated carbons derived from carbonized coconut shell chars, Ind. Crop. Prod. 28 (2) (2008) 190–198, https://doi.org/10.1016/j.indcrop.2008.02.012.
[128] S. Guo, J. Peng, W. Li, K. Yang, L. Zhang, S. Zhang, H. Xia, Effects of CO2 activation on porous structures of coconut shell-based activated carbons, Appl. Surf. Sci. 255 (20) (2009) 8443–8449, https://doi.org/10.1016/j.apsusc.2009.05.150.
[129] O.-W. Achaw, G. Afrane, The evolution of the pore structure of coconut shells during the preparation of coconut shell-based activated carbons, Microporous Mesoporous Mater. 112 (1–3) (2008) 284–290, https://doi.org/10.1016/j.micromeso.2007.10.001.
[130] M. Borghei, N. Laocharoen, E. Kibena-Põldsepp, L.-S. Johansson, J. Campbell, E. Kauppinen, K. Tammeveski, O.J. Rojas, N. Porous, P-doped carbon from coconut shells with high electrocatalytic activity for oxygen reduction: alternative to Pt-C for alkaline fuel cells, Appl. Catal., B 204 (2017) 394–402, https://doi.org/10.1016/j.apcatb.2016.11.029.
[131] H. Wang, J. Sun, J. Wang, L. Jiang, H. Liu, Green synthesis of nitrogen and fluorine co-doped porous carbons from sustainable coconut shells as an advanced synergistic electrocatalyst for oxygen reduction, J. Mater. Res. Technol. 13 (2021) 962–970, https://doi.org/10.1016/j.jmrt.2021.05.048.
[132] Y. Sun, Y. Duan, L. Hao, Z. Xing, Y. Dai, R. Li, J. Zou, Cornstalk-derived nitrogen-doped partly graphitized carbon as efficient metal-free catalyst for oxygen reduction reaction in microbial fuel cells, ACS Appl. Mater. Interfaces 8 (39) (2016) 25923–25932, https://doi.org/10.1021/acsami.6b06895.
[133] W. Wan, Q. Wang, L. Zhang, H.-W. Liang, P. Chen, S.-H. Yu, N-, P- and Fe-tridoped nanoporous carbon derived from plant biomass: an excellent oxygen reduction electrocatalyst for zinc–air batteries, J. Mater. Chem. 4 (22) (2016) 8602–8609, https://doi.org/10.1039/c6ta02150f.
[134] Z. Yan, M. Zhang, J. Xie, H. Wang, W. Wei, Smaller Pt particles supported on mesoporous bowl-like carbon for highly efficient and stable methanol oxidation and oxygen reduction reaction, J. Power Sources 243 (2013) 48–53, https://doi.org/10.1016/j.jpowsour.2013.06.008.
[135] M. Liu, W. Chen, Green synthesis of silver nanoclusters supported on carbon nanodots: enhanced photoluminescence and high catalytic activity for oxygen reduction reaction, Nanoscale 5 (24) (2013) 12558–12564, https://doi.org/10.1039/c3nr04054b.
[136] M. Wassner, M. Eckardt, C. Gebauer, G.R. Bourret, N. Hüsing, R.J. Behm, Synthesis and electrocatalytic performance of spherical core-shell tantalum (oxy) nitride@nitrided carbon composites in the oxygen reduction reaction, Electrochim. Acta 227 (2017) 367–381, https://doi.org/10.1016/j.electacta.2016.12.145.
[137] N. Brun, S.A. Wohlgemuth, P. Osiceanu, M.M. Titirici, Original design of nitrogen-doped carbon aerogels from sustainable precursors: application as metal-free oxygen reduction catalysts, Green Chem. 15 (9) (2013), https://doi.org/10.1039/c3gc40904j.
[138] S.-M. Alatalo, K. Qiu, K. Preuss, A. Marinovic, M. Sevilla, M. Sillanpää, X. Guo, M.-M. Titirici, Soy protein directed hydrothermal synthesis of porous carbon aerogels for electrocatalytic oxygen reduction, Carbon 96 (2016) 622–630, https://doi.org/10.1016/j.carbon.2015.09.108.
[139] Y. Qiu, J. Huo, F. Jia, B.H. Shanks, W. Li, N- and S-doped mesoporous carbon as metal-free cathode catalysts for direct biorenewable alcohol fuel cells, J. Mater. Chem. 4 (1) (2016) 83–95, https://doi.org/10.1039/c5ta06039g.
[140] G.-L. Li, C.-D. Liu, S.-M. Chen, C. Hao, G.-C. Cheng, Y.-Y. Xie, Promotion of oxygen reduction performance by Fe3O4 nanoparticles support nitrogen-doped three dimensional meso/macroporous carbon based electrocatalyst, Int. J. Hydrogen Energy 42 (7) (2017) 4133–4145, https://doi.org/10.1016/j.ijhydene.2016.10.081.
[141] Q. Lai, Q. Su, Q. Gao, et al., In situ self-sacrificed template synthesis of Fe-N/G catalysts for enhanced oxygen reduction, ACS Appl. Mater. Interfaces 7 (32) (2015) 18170–18178. https://pubs.acs.org/doi/abs/10.1021/acsami.5b05834.
[142] J. Yang, J. Hu, M. Weng, R. Tan, L. Tian, J. Yang, J. Amine, J. Zheng, H. Chen, F. Pan, Fe-cluster pushing electrons to N-doped graphitic layers with Fe_3C(Fe) hybrid nanostructure to enhance O_2 reduction catalysis of Zn-air batteries, ACS Appl. Mater. Interfaces 9 (5) (2017) 4587–4596, https://doi.org/10.1021/acsami.6b13166.
[143] Q. Zhao, Q. Ma, F. Pan, Z. Wang, B. Yang, J. Zhang, J. Zhang, Facile synthesis of nitrogen-doped carbon nanosheets as metal-free catalyst with excellent oxygen reduction performance in alkaline and acidic media, J. Solid State Electrochem. 20 (5) (2016) 1469–1479, https://doi.org/10.1007/s10008-016-3157-z.
[144] K. Cheng, Z. Kou, J. Zhang, M. Jiang, H. Wu, L. Hu, X. Yang, M. Pan, S. Mu, Ultrathin carbon layer stabilized metal catalysts towards oxygen reduction, J. Mater. Chem. 3 (26) (2015) 14007–14014, https://doi.org/10.1039/c5ta02386f.
[145] Y. Li, H. Zhang, P. Liu, Y. Wang, H. Yang, Y. Li, H. Zhao, Self-supported bimodal-pore structured nitrogen-doped carbon fiber aerogel as electrocatalyst for oxygen reduction reaction, Electrochem. Commun. 51 (2015) 6–10, https://doi.org/10.1016/j.elecom.2014.11.020.
[146] X. Wu, S. Li, B. Wang, J. Liu, M. Yu, From biomass chitin to mesoporous nanosheets assembled loofa sponge-like N-doped carbon/g-C_3N_4 3D network architectures as ultralow-cost bifunctional oxygen catalysts, Microporous Mesoporous Mater. 240 (2017) 216–226, https://doi.org/10.1016/j.micromeso.2016.11.022.
[147] K. Preuss, V.K. Kannuchamy, A. Marinovic, M. Isaacs, K. Wilson, I. Abrahams, M.-M. Titirici, Bio-inspired carbon electro-catalysts for the oxygen reduction reaction, J. Energy Chem. 25 (2) (2016) 228–235, https://doi.org/10.1016/j.jechem.2016.01.001.
[148] H. Yuan, L. Deng, X. Cai, S. Zhou, Y. Chen, Y. Yuan, Nitrogen-doped carbon sheets derived from chitin as non-metal bifunctional electrocatalysts for oxygen reduction and evolution, RSC Adv. 5 (69) (2015) 56121–56129, https://doi.org/10.1039/c5ra05461c.
[149] B. Zhang, C. Wang, D. Liu, Y. Liu, X. Yu, L. Wang, Boosting ORR electrocatalytic performance of metal-free mesoporous biomass carbon by synergism of huge specific surface area and ultrahigh pyridinic nitrogen doping, ACS Sustain. Chem. Eng. 6 (11) (2018) 13807–13812, https://doi.org/10.1021/acssuschemeng.8b01876.
[150] J. Zhao, Y. Liu, X. Quan, S. Chen, H. Yu, H. Zhao, Nitrogen-doped carbon with a high degree of graphitization derived from biomass as high-performance electrocatalyst for oxygen reduction reaction, Appl. Surf. Sci. 396 (2017) 986–993, https://doi.org/10.1016/j.apsusc.2016.11.073.
[151] J. Tong, W. Ma, W. Wang, J. Ma, W. Li, L. Bo, H. Fan, Nitrogen/phosphorus dual-doped hierarchically porous graphitic biocarbon with greatly improved performance on oxygen reduction reaction in alkaline media, J. Electroanal. Chem. 809 (2018) 163–170, https://doi.org/10.1016/j.jelechem.2017.12.055.

[152] W. Liang, J. Chen, Y. Liu, S. Chen, Density-functional-theory calculation analysis of active sites for four-electron reduction of O2 on Fe/N-doped graphene, ACS Catal. 4 (11) (2014) 4170–4177, https://doi.org/10.1021/cs501170a.
[153] G. Wu, K.L. More, C.M. Johnston, P. Zelenay, High-performance electrocatalysts for oxygen reduction derived from polyaniline, iron, and cobalt, Science 332 (6028) (2011) 443–447, https://doi.org/10.1126/science.1200832.
[154] Y. Zhang, L. Lu, S. Zhang, Z. Lv, D. Yang, J. Liu, Y. Chen, X. Tian, H. Jin, W. Song, Biomass chitosan derived cobalt/nitrogen doped carbon nanotubes for the electrocatalytic oxygen reduction reaction, J. Mater. Chem. 6 (14) (2018) 5740–5745, https://doi.org/10.1039/c7ta11258k.
[155] X. Liu, I.S. Amiinu, S. Liu, K. Cheng, S. Mu, Transition metal/nitrogen dual-doped mesoporous graphene-like carbon nanosheets for the oxygen reduction and evolution reactions, Nanoscale 8 (27) (2016) 13311–13320, https://doi.org/10.1039/c6nr03247h.
[156] N. Han, S. Wang, A. Rana, et al., Rational design of boron nitride based materials for sustainable applications, Renew. Sust. Energ. Rev. 17 (2022), 112910, https://doi.org/10.1016/j.rser.2022.112910.
[157] Q. Wang, N. Han, Z. Shen, et al., MXene-based electrochemical (bio) sensors for sustainable applications: roadmap for future advanced materials, Nano Mater. Sci. (2022), https://doi.org/10.1016/j.nanoms.2022.07.003.
[158] Q. Wang, N. Han, A. Bokhari, et al., Insights into MXenes-based electrocatalysts for oxygen reduction, Energy 255 (2022), 124465, https://doi.org/10.1016/j.energy.2022.124465.